EVALUATION OF CORROSION RESISTANCE OF TYPE 304 STAINLESS STEEL CLAD REINFORCING BARS

By
Jason T. Kahrs
David Darwin
Carl E. Locke, Jr.

A Report on Research Sponsored by

THE NATIONAL SCIENCE FOUNDATION
Research Grant No. CMS - 9812716

KANSAS DEPARTMENT OF TRANSPORTATION
Contract No. C1131

STRUCTURAL METALS, INC.

Structural Engineering and Engineering Materials
SM Report No. 65
August 2001

THE UNIVERSITY OF KANSAS CENTER FOR RESEARCH, INC.
2385 Irving Hill Drive - Campus West, Lawrence, Kansas 66044

EVALUATION OF CORROSION RESISTANCE OF TYPE 304 STAINLESS STEEL CLAD REINFORCING BARS

By

Jason T. Kahrs

David Darwin

Carl E. Locke, Jr.

A Report on Research Sponsored by

THE NATIONAL SCIENCE FOUNDATION
Research Grant No. CMS - 9812716

KANSAS DEPARTMENT OF TRANSPORTATION
Contract No. C1131

STRUCTURAL METALS, INC.

Structural Engineering and Engineering Materials
SM Report No. 65

THE UNIVERSITY OF KANSAS CENTER FOR RESEARCH, INC.

August 2001

ABSTRACT

The corrosion performance of a prototype 304 stainless steel clad reinforcing bar and conventional reinforcing steel is compared based on corrosion potential and macrocell corrosion tests. Tests are conducted on bare bars and bars symmetrically embedded in a mortar cylinder. Test specimens consist of bars with ends protected with epoxy or with plastic caps filled with epoxy, and clad bars with a hole drilled through the cladding. Specimens are exposed to a simulated concrete pore solution with a 1.6 molal ion concentration of sodium chloride. Additional corrosion potential tests include specimens exposed to simulated concrete pore solution with and without pressurized air pumped into the solution and a conventional bar with a reduced thickness of mortar cover. Additional macrocell corrosion tests include sandblasted stainless steel clad bars, damaged stainless steel specimens connected to conventional steel cathodes, mortar covered conventional bars connected to bare conventional bars, and specimens with a reduced thickness of mortar. The thickness and uniformity of the stainless steel cladding is evaluated using a scanning electron microscope.

The results indicate the prototype 304 stainless steel clad reinforcement exhibits superior corrosion resistance compared to conventional reinforcing steel, but requires adequate protection at cut ends, where the mild steel core is not covered by cladding. For bare stainless steel clad bars, the macrocell corrosion rate varies between 0.0 to 0.3 μm/yr (0.0 to 0.012 mpy), about $^{1}/_{100}$ of the value observed for conventional bars. Stainless steel bars embedded in mortar exhibit corrosion rates between 0.0 and 0.2 μm/yr (0.0 and 0.008 mpy), averaging $^{1}/_{20}$ to $^{1}/_{50}$ of the value exhibited by conventional bars. The corrosion rates for clad bars with a drilled hole through the cladding range between 0.0 and 0.75 μm/yr (0.0 and 0.03 mpy), averaging about $^{1}/_{70}$ of the value exhibited by conventional steel bars. The thickness of the stainless steel cladding on bars in the current study varies between 0.196 to 0.894 mm (7.7 to 35 mils). Imperfections in the form of an indentation in the base material and a crack in the cladding material filling the indention were observed. The

crack did not penetrate the stainless steel cladding and cladding is of adequate thickness to protect the mild steel core. Longer-term tests are recommended, as is use of the bar in demonstration bridge decks.

Key words: chlorides; clad reinforcement; concrete; corrosion; macrocell; potential; reinforcing bars; type 304 stainless steel

ACKNOWLEDGEMENTS

This report is based on a thesis submitted by Jason T. Kahrs in partial fulfillment of the requirements of the MSCE degree. Major funding and material support for this research was provided by the National Science Foundation under NSF Grant No. CMS - 9812716, the Kansas Department of Transportation under Contract No. C1131, and Structural Metals, Inc. Additional support for this project was provided by Dupont Corporation, 3M Corporation, and LRM Industries. Oversight for the project was provided by Dan Scherschligt of the Kansas Department of Transportation.

TABLE OF CONTENTS

LIST OF TABLES

LIST OF FIGURES

CHAPTER 1
INTRODUCTION

1.1 General

Corrosion of concrete reinforcement can be a major problem when concrete is continually subjected to deicing chemicals or saltwater. The cost of corrosion damage caused by deicing salts on reinforced concrete bridge decks and car parking structures has been estimated to cost the United States between $325 and $1000 million/year (NRC 1991). For this reason, several methods are under study to protect reinforcing steel.

Numerous methods have been developed to reduce or halt the damage to reinforcing steel caused by corrosion. One method is to apply an effective, economical coating over conventional steel to make it less susceptible to corrosion. Epoxy-coated bars, galvanized reinforcement, and metal cladding represent techniques that have been used. Epoxy-coated reinforcing steel constitutes the majority of the protected steel currently used in bridge decks across the United States. The epoxy acts as a barrier, keeping oxygen, moisture, and chloride ions from reaching the surface of the steel, and increases the electrical resistance between adjacent bars. Major concerns with epoxy coatings are their ability to withstand inadvertent damage caused by shipping and handling, and their tendency to soften and lose adhesion in a moist environment. Galvanized bars are protected because the zinc acts as both a barrier and a sacrificial coating, corroding in place of the conventional steel core. The corrosion products, however, increase in volume and may cause the concrete to crack. Metal claddings, such as copper, nickel, and stainless steel, protect conventional steel due to the inherent corrosion resisting properties of the cladding material. Research and practical applications of metallic coatings have shown that the coatings significantly reduce the corrosion rate of reinforcing steel. The use of metal clad reinforcing steel has been limited in the United States because of high initial costs of construction, and in the case of copper, due to damage to the surrounding concrete.

The purpose of this study is to compare the corrosion performance of a prototype 304 stainless steel clad bar to that of conventional (black) reinforcing steel.

1.2 Background

Concrete is a material that contains numerous pores and microcracks, which allow both moisture and oxygen to migrate through the concrete to the surface of reinforcing bars. Steel will be protected from corrosion if the alkalinity, pH, of the concrete pore solution remains above 11.5 – the usual case. High levels of sodium and potassium hydroxide in the pore solution contribute to a high alkalinity (Revie 2000). A highly alkaline environment passivates the steel and results in the formation of a dense γ ferric oxide film. The film isolates the metal from the pore solution and reduces the ability of iron to go into solution, thus halting corrosion. Chlorides and carbon dioxide, however, can destroy the passivating film. Chlorides cause iron to go into solution, while carbon dioxide lowers the pH of the concrete pore solution.

Contamination and ingress are two ways that chlorides can be introduced to concrete. Contamination can be caused by deliberate additions of calcium chloride set accelerators or seawater to the mix or by the accidental use of inadequately washed marine sourced aggregates. Deicing salts and seawater result in ingress of chlorides into concrete. In most cases, a chloride level of 0.4% chloride by weight of cement is a necessary but not sufficient condition for corrosion. Under conditions of variable chloride contents and aggressive environments, corrosion may occur at $\approx$ 0.2% chloride by weight of cement (ACI Committee 222 1996).

Chloride ingress into concrete is generally believed to follow Fick's second law of diffusion.

$$d[Cl^-]/dt = D_c \cdot d^2[Cl^-]/dx^2 \qquad (1.1)$$

where $[Cl^-]$ is the chloride concentration, at depth x and time t, and D_c is the diffusion coefficient. Where chlorides diffuse in from a surface, the following solution to the differential equation can be used to model the system.

$$(C_{max} - C_{x,t})/(C_{max} - C_{min}) = \text{erf} \bullet x/((4D_c t)^{0.5})) \qquad (1.2)$$

where

C_{max} is the surface or near surface concentration

$C_{x,t}$ is the chloride concentration at depth x at time t

C_{min} is the background chloride concentration

erf is the error function

The parameter C_{max} must be a constant, which is why a near surface measurement is used. This prevents fluctuations in surface levels on wetted and dried surfaces.

Chloride ions contribute to the removal of the passivating iron-oxide film by combining with iron cations located on the surface of the reinforcing bar, creating an iron-chloride complex. When hydroxyl ions are exposed to iron-chloride, they react to form ferrous hydroxide, releasing the chloride ions back into solution. Consequently, the passive iron-oxide film is dissolved.

$$Fe^{++} + 2Cl^{-} \rightarrow FeCl_2 + 2e^{-} \qquad (1.3)$$

$$FeCl_2 + 2OH^{-} \rightarrow Fe(OH)_2 + 2Cl^{-} \qquad (1.4)$$

Carbon dioxide also contributes to the corrosion of reinforcing steel by reacting with the concrete pore water to form carbonic acid. Carbonic acid reacts with the calcium and alkali hydroxides to form solid carbonates, causing the pH of the concrete to drop from pH $\approx$ 13 to pH $\approx$ 8. The passive oxide layer is lost once the pH drops below about 11.5.

Low concrete cover, poor concrete quality, poor consolidation, and old age are factors commonly associated with carbonation. Carbonated concrete may be good quality concrete, but the steel is no longer protected from corrosion by a passivating film. Carbonation rates generally follow parabolic kinetics.

$$d = A\, t^{0.5} \qquad (1.5)$$

where d = carbonation depth

t = time

A is a constant, generally on the order 0.25 to 1.0 mm/year$^{1/2}$

The time it takes carbon dioxide to reach the steel can be decreased by wet/dry cycling. A sufficient amount of moisture is also required to cause corrosion.

The research presented is this paper is focused on chloride attack, which can develop in concrete when roadway deicers are used or in marine environments.

1.3 Electrochemistry

Electrochemistry is based on the principles of mixed potential theory. Mixed potential theory separates the oxidation and reduction reactions that occur on a corroding surface, and postulates that the total rates of all oxidation reactions equal the total rates of all reduction reactions (Sedriks 1996). For corrosion of steel in concrete, the electrochemical process begins with the formation of a galvanic cell (similar to a battery). A galvanic cell, or electrochemical cell, is made up of two electrodes, generally of different composition, that are immersed in an aqueous solution (electrolyte) and connected by an electrical conductor (Beddoes and Parr 1999). A shift in energy (potential) between the electrodes leads to the instigation of oxidation and reduction reactions. Shifts are generally caused by bar imperfections and/or different concentrations of chloride ions, oxygen, moisture, or hydroxyl ions in the concrete pore solution surrounding the electrodes. Oxidation occurs at the more positively charged electrode (anode). For steel, an iron alloy, a possible reaction is the oxidation of the iron component. Ferrous ions are dissolved into the electrolyte and free electrons are available to flow through the steel.

$$\underset{\text{Iron}}{Fe} \rightarrow \underset{\text{Ferrous Ion}}{Fe^{++}} + \underset{\text{2 Electrons}}{2e^-} \qquad (1.6)$$

The electrons deposited on the surface of the steel cause the potential of the anode to drop. As the potential difference between the electrodes increases, the electrons leave the anode and naturally flow through the electrical conductor to the more negatively charged electrode (cathode), where a reduction reaction takes place in which the electrons combine with oxygen and water to form hydroxyl ions.

$$\underset{\text{Oxygen}}{\tfrac{1}{2} O_2} + \underset{\text{Water}}{H_2O} + \underset{\text{2 Electrons}}{2e^-} \rightarrow \underset{\text{2 Hydroxyl Ions}}{2 (OH^-)} \qquad (1.7)$$

If steel is corroding in concrete, the hydroxyl ions will migrate to the anode through the liquid located in the concrete pores and capillaries. The hydroxyl ions combine with iron cations at the anode and form hydrous iron oxides (rust) [Eq. (1.8)]. Red rust (ferric oxide) is a type of rust that can develop when ferrous hydroxides react with water and oxygen [Eq. (1.9)]. Black rust may occur if iron reacts directly with hydroxyl ions to produce iron oxide, water, and free electrons [Eq. (1.10)].

$$Fe^{++} + 2 (OH^-) \rightarrow Fe(OH)_2 \qquad (1.8)$$

$$4 Fe(OH)_2 + 2 H_2O + O_2 \rightarrow 4 Fe(OH)_3 \qquad (1.9)$$

$$3 Fe + 8 OH^- \rightarrow Fe_3O_4 + 8 e^- + 4 H_2O \qquad (1.10)$$

By eliminating water, oxygen, or electron flow between the electrodes, corrosion of reinforcing steel can be stopped. Whether or not steel will corrode depends on the thermodynamics of the electrochemical processes. Pourbaix diagrams are calculated potential versus pH diagrams that show the most stable phase of a metal in various specific aqueous environments. Pourbaix diagrams are valid only for pure elements in specific conditions (e.g., T = 25 °C and p = 1 atm), and show the reactions

and reaction products present when the potential of the reduction and oxidation reactions occurring at the metal/solution interface are in equilibrium. The diagrams are divided by boundary lines, derived from the Nernst equation, into several regions where different phases of the elements are stable. Fig. 1.1 shows a simplified Pourbaix diagram for the Fe-H_2O (pure water) system. The diagram is divided into corrosive, immune, and passive regions. In the corrosive region, the most stable form of the metal is the ferrous ion. Corrosion will occur until the metal is consumed. The immune region represents an area where corrosion is thermodynamically impossible. In the passive region, an insoluble protective layer is the most stable form. Initial corrosion will occur until the protective layer is formed.

For steel in concrete, the pH is in the range of 13 to 13.5. Steel in concrete without chlorides present has a potential of about –0.2 V with respect to the standard calomel cell (SCE) [+0.042 V versus standard hydrogen electrode (SHE)], a value in the passive region.

The thermodynamics of the corrosion process only predict if the reactions will take place. The kinetics of the corrosion process depends on the quantity of electrons produced or consumed by electrochemical reactions. The transfer of charge between the reactions is defined in terms of the charge per unit area per unit time or current density.

The driving force in electrochemical cells is the potential difference between the anode and cathode. Variances in potential along a single bar lead to the formation of miniature galvanic cells, called microcells. Electrochemical cells that develop between two bars or layers of bars are called macrocells. Macrocells can develop in bridge decks when chloride ions from roadway deicers penetrate the concrete to the level of the top mat of reinforcing steel. Potential differences will occur because the chloride ions alter the environment surrounding the top mat, while the environment surrounding the bottom mat remains largely unchanged. Both microcell and macrocell corrosion typically occur in the top mat of bridge deck reinforcement, where chlorides introduced by deicing salts, moisture, and oxygen are readily available.

1.4 Rapid Electrochemical Corrosion Tests

The corrosion potential and macrocell tests performed in this study are based on previous research at the University of Kansas (Martinez, Darwin, McCabe, and Locke 1990, Schwensen, Darwin, and Locke 1995, Senecal, Darwin, and Locke 1995). The experimental program consists of tests performed on both plain reinforcing bars and bars embedded in a cylinder of mortar. A schematic of a test specimen with the reinforcing bar embedded in mortar is shown in Fig. 1.3. For this study, a 127 mm (5 in.) long No. 19 [No. 6] bar is symmetrically embedded 76 mm (3 in.) in a 38 mm (1.5 in.) diameter mortar cylinder. This differs from earlier studies in which a No. 16 [No. 5] bar was embedded in a 30 mm (1.18 in.) diameter mortar cylinder. To prevent crevice corrosion, two layers of epoxy are placed around the region of the bar that protrudes from the mortar. The length of the cylinders is 102 mm (4 in.), making the overall specimen length 153 mm (6 in.). The mortar has a water/cement ratio of 0.5 and a sand/cement ratio of 2. The mortar is made with Type I portland cement, deionized water, and standard graded Ottawa sand meeting the requirements of ASTM C 778.

The *potential test* measures the corrosion potential of the specimen exposed to an aqueous alkali chloride solution. Potential readings are recorded on a daily basis for 40 days. The measurements are taken with respect to a saturated calomel electrode (SCE) submerged in a saturated potassium chloride solution. A schematic of the test is shown in Fig. 1.4. A specimen is placed in a plastic container filled with an electrolyte, which is comprised of a simulated concrete pore solution (Farzammehr 1985) with a 1.6 m ion concentration of sodium chloride. A salt bridge ionically connects the specimen container with the container holding the SCE.

The *macrocell test* measures the macrocell corrosion rate that exists between one anodic and two cathodic test specimens (Fig. 1.5). The anode is placed in a container similar to that of the potential test specimen. The cathodic bars are placed in a separate container filled with only simulated concrete pore solution. Air (scrubbed to

remove CO_2) is bubbled into the pore solution to ensure an adequate supply of oxygen at the cathode. The solutions at the anode and cathode are connected with a salt bridge. Copper wiring is used to electrically connect the anode and cathodes across a 10 ohm resistor. The corrosion current is calculated after measuring the voltage drop across the resistor. The corrosion current is then converted to rate of metal loss using Faraday's law.

$$m = (i \cdot a)/(n \cdot F \cdot D) \qquad (1.11)$$

where m = depth of metal loss per year (μm/yr)

i = current density of the macrocell (mA/cm^2)

a = atomic weight of the metal (55.84 grams/gram-atom for iron)

n = number of ion equivalents exchanged (2 for $Fe \rightarrow Fe^{++} + 2e^-$)

F = Faraday's constant (96,500 coulombs/equivalent)

D = density of the metal (7.87 grams/cm^3 for iron)

The current density is determined by dividing the current (obtained from the voltage drop) by the surface area of the anodic bar. The surface area is calculated by treating the bar as a cylinder. Voltage measurements are taken daily for 100 days.

1.5 Corrosion-Monitoring Methods

The following methods may be used to monitor the degree of corrosion in the rapid tests.

1.5.1 Visual Inspection

A visual inspection of the test specimens will give an early indication of the extent of corrosion. Inspections typically entail a survey and log of every defect seen

on the surface of the bar. Surveys must be followed up by testing to confirm the source and cause of deterioration. The main limitation of visual surveys is the skill and experience of the inspector.

1.5.2 Electrochemical Potential Measurements

Electrochemical potential measurements of steel with respect to a standard reference electrode indicate the corrosion "state" of the steel. The absolute potential, or energy, of a metal cannot be measured directly. However, the potential difference between two chemical reactions can be measured directly. Reference electrodes contain materials that undergo known chemical reactions. The chemical reaction that has been chosen to have zero potential with respect to all other chemical reactions is $2H^+ + 2e^- \rightleftarrows H_2$, which occurs in the standard hydrogen electrode (SHE). The relationship between the SHE and other types of standard reference electrodes is shown in Table 1.1. Small differences in the potential values as shown in Table 1.1 (on the order of a few millivolts) are reported by different references.

The copper/copper sulfate electrode (CSE) is widely used to measure the potential of steel in bridge decks. ASTM C 876 is the standard test method for determining the corrosion potential of uncoated bars in concrete using the CSE (ASTM C 876).

The corrosion state of steel can be classified as passive, active, or indeterminate, depending on the difference in potential between the steel and reference electrode. The potential difference is determined by setting up an electrochemical cell between the steel and a reference electrode, and measuring the voltage drop between the electrodes using a voltmeter.

The ranges of potential values that signify a high or low corrosion risk for steel in concrete have been determined in previous studies (Page and Treadway 1992, Schiessl 1988, Clear 1989). A potential range between +100 mV to –200 mV (versus SCE) indicates that the steel is in a non-corroding, passive state. Corrosion potentials between –200 mV and –500 mV (versus SCE) imply localized corrosion is occurring,

and potentials between –450 mV and –600 mV (versus SCE) indicate a good probability that general corrosion is underway.

ASTM C 876 states that a corrosion potential more negative than –350 mV versus CSE (-273 mV versus SCE) has a greater than 90% probability that reinforcing steel corrosion is occurring in that area at the time of measurement. If the potential is more positive than –200 mV versus CSE (-123 mV versus SCE), there is a greater than 90% probability that no reinforcing steel corrosion is occurring in that area at the time of measurement. For values between –200 mV and –350 mV, the corrosion activity is uncertain. In general, reinforcing steel is considered passive at potentials more positive than -200 mV (versus SCE).

1.5.3 Corrosion Rate Measurement

Another method used to monitor corrosion is to measure the rate of macrocell corrosion. The macrocell corrosion rate may be determined by measuring the voltage drop across a resistor placed in series with the electron path between an anode and cathode. Measuring the rate of macrocell corrosion can be difficult to perform due to limited access to the reinforcing steel in concrete structures. However, measuring the corrosion rate of macrocells is well suited for laboratory studies, where specially designed specimens can be used. A typical laboratory macrocell test entails creating an electrochemical cell, and connecting a resistor between the anode and cathode specimens (Fig. 1.5). The depth of metal loss per year at the anode can be estimated using Eq. (1.11).

The rate of corrosion can also be determined using the linear (resistance) polarization technique. At potentials very close to corrosion potential, E_{corr}, ± 10 mV, the potential versus corrosion current is approximately linear, as shown in Fig. 1.6.

The relationship between the corrosion current density, I_{corr}, and the slope, $\Delta E/\Delta I$, can be shown to be

$$I_{corr} = [\beta_a \beta_c / (2.3(\beta_a + \beta_c))]\ \Delta I/\Delta E \qquad (1.12)$$

where β_a and β_c are the anodic and cathodic Tafel slopes, respectively (Stearn and Geary 1957, Stearn and Weisert 1959). The quantity $\beta_a\beta_c/ (2.3(\beta_a + \beta_c))$ is generally accepted as a constant, making the equation for corrosion current density (Stern and Geary 1985):

$$I_{corr} = B / R_p \qquad (1.13)$$

where I_{corr} = the corrosion current density ($\mu A/cm^2$)

$B = \beta_a\beta_c/ (2.3(\beta_a + \beta_c))$ (often taken as 26 mV for reinforced concrete)

and R_p = the polarization resistance = $\Delta I/\Delta E$

where ΔI = incremental change in current

ΔE = incremental change in potential

Polarization measuring devices that include a guard ring around the auxiliary electrode have shown good performance in field and laboratory trials for reinforced concrete. The guard ring allows for a more accurately defined area of measurement than devices without a ring. The following broad criteria for corrosion have been developed from field and laboratory investigations using a sensor controlled guard ring device (Broomfield, Rodriguez, Ortega, and Garcia 1993).

$I_{corr} < 0.1\ \mu A/cm^2$	Passive condition
$I_{corr} = 0.1 - 0.5\ \mu A/cm^2$	Low to moderate corrosion
$I_{corr} = 0.5 - 1\ \mu A/cm^2$	Moderate to high corrosion
$I_{corr} > 1\ \mu A/cm^2$	High corrosion rate

These values can be affected by temperature and relative humidity. Therefore, conditions at the time of measurement need to be considered when interpreting

the limits defined above. A value of 26 mV was used for the constant B (Eq. 1.13) to determine the above criteria. For devices without a guard ring, the constant B is typically taken as 52 mV.

The amount of expansive oxide (rust) growth to cause cracking in concrete is between 10 and 100 μm (0.4 and 4 mils). The increase in volume of oxides produced by steel may be two to six times the steel consumed. Assuming an average oxide expansion ratio of 3, the corrosion rates given above translate as follows:

0.1 $\mu A/cm^2$ = 1.1 μm/yr section loss ≈ 3 μm/yr rust growth

0.5 $\mu A/cm^2$ = 5.7 μm/yr section loss ≈ 17.3 μm/yr rust growth

1 $\mu A/cm^2$ = 11.5 μm/yr section loss ≈ 34 μm/yr rust growth

1.6 PREVIOUS WORK

Commercial applications of iron-base alloys containing chromium (12%+ Cr) where first used in 1912 by Harry Brearly (Larkin 1966). Brearly observed the superior corrosion resistance of the alloys and later named these ferritic metals "stainless steel." Around the same time, Maurer and Strauss (Maurer 1933) produced an austenitic stainless steel that contained about 8% nickel. The factors leading to passivity of various stainless steels were first investigated by Monnartz (1911) in his doctoral research. Between 1925 and 1935, ferritic and austenitic stainless steels were being used on a large-scale in England, Germany, and the United States in ammonia and nitric acid plants. Since that period, production of austenitic stainless steels in the United States has almost doubled in volume compared to that of ferritic alloys. The majority of stainless steels are used by the chemical, petroleum, process, and power industries. The initial project costs associated with using stainless steel have limited its use in highway structures.

In recent years, several research projects have been conducted to compare corrosion properties of stainless steel and stainless steel clad reinforcement to conventional steel. In 1985, Zoob, LeClaire, and Pfeifer conducted cyclic corrosion tests

using type 304 solid stainless steel deformed reinforcing bars. In that study, two mats of 12 mm (0.5 in.) diameter bars were cast into concrete slabs and electrically connected. A 15 % chloride solution was ponded on the slabs. The slab specimens were ponded for 4 days at 16 to 27 °C (61 to 81 °F), rinsed, and dried for three days at 38 °C (100 °F). The wetting/drying process was repeated for 48 weeks. The results of the tests showed that slabs with conventional ASTM A 615 bars generated an average maximum corrosion current density of about 9.6 mA/m^2 with respect to the steel surface area (equivalent to metal loss of 111 μm/yr (4.37 mils/yr)). These bars exhibited severe corrosion and caused cracks in the concrete. Slabs with stainless steel exhibited no measurable macrocell corrosion current during the 48 weeks of testing.

Sorensen, Jensen, and Maahn (1990) compared the corrosion performance of type 304 and 316 stainless steels with that of conventional steel. The electrochemical investigation found that the Cl^- content threshold for corrosion to occur for reinforcing bars embedded in mortar with admixed chloride was more that 10 times higher for stainless than for conventional steel. The critical chloride content by weight of cement was less than 0.5 percent of admixed chloride for the conventional steel, while the critical chloride content for 304 stainless steel was 5 to 8 percent and greater than 8 percent for type 316 stainless steel.

Type 304 stainless clad bars were tested by Rasheeduzzafar, Bader, and Khan (1992) over a period of 7 years. Stainless clad and mild steel bars were embedded in concrete containing 19.2 kg/m^3 (32.4 lb/yd^3) of admixed chloride ion. All of the conventional steel specimens showed severe concrete cracking, while the stainless steel clad specimens exhibited no sign of corrosion or damage to the concrete. It was concluded that the chloride ion threshold for the clad bars was more than 24 times greater than the accepted corrosion threshold for conventional steel in concrete.

A nine-year field study was performed on a bridge deck constructed for the New Jersey Department of Transportation that contained 304 stainless steel clad reinforcing bars produced in England (McDonald, Sherman, Pfeifer, and Virmani 1995). Four cores were removed from the bridge deck. The cores contained nine stainless-

clad bars. These bars showed no corrosion on the surface of the steel. Corrosion, however, was observed under the plastic end caps on the bars, where the conventional steel core was not coated with stainless steel.

In 1998, McDonald, Pfeifer, and Sherman reported the results of a five-year study on the corrosion performance of solid 304 and 316 stainless steels. In that study, the lowest corrosion rates of the 304 stainless steel bars were obtained when the stainless bars acted as both the anode and cathode. The test results indicated that the 304 stainless steel bars were about 1500 times less corrosive than the conventional bar specimens. However, when the stainless steel cathode was replaced with a conventional steel cathode, five out of ten of the 304 stainless bars exhibited moderate to high corrosion currents. A visual inspection showed that two of the stainless steel bars that had conventional steel cathodes and were near a precracked location of the concrete had moderate red rust corrosion. No corrosion staining was observed when stainless cathodes were used. The 316 bars had about 800 times less corrosion than conventional steel, and were little affected by galvanic effects when used in conjunction with conventional bars as cathodes.

1.7 OBJECTIVE AND SCOPE

Corrosion potential and macrocell corrosion tests are performed to compare the corrosion properties of conventional and type 304 stainless steel clad reinforcing bars. Test specimens are exposed to simulated concrete pore solution with a 1.6 molal (m) ion concentration of sodium chloride. The tests are conducted on bare and mortar covered specimens. The ends of the steel bars are protected with either epoxy coatings or plastic caps filled with epoxy.

Corrosion potential tests performed on bare conventional and stainless steel clad specimens include six bars with the ends protected with an epoxy coating, two with the ends protected by a cap filled with epoxy, two clad bars with a hole drilled through the cladding, two bars exposed to simulated pore solution without NaCl, and

two bars exposed to simulated pore solution without NaCl and with air, scrubbed to remove CO_2, bubbled into the solution.

Corrosion potential tests conducted on conventional and stainless steel clad bars embedded in mortar include six bars with the ends protected with an epoxy coating, three with the ends protected by a cap filled with epoxy, and one conventional bar with a reduced mortar cover.

Macrocell corrosion tests performed on bare conventional and stainless steel clad specimens include six bars with the ends protected with an epoxy coating, three with the ends protected by a cap filled with epoxy, two sandblasted clad bars, three clad bars with a hole drilled through the cladding, and three clad bars with a hole drilled through the cladding connected to conventional steel cathodes.

Macrocell corrosion tests conducted on conventional and stainless steel clad bars embedded in mortar include nine conventional bars with the ends protected with an epoxy coating, six clad bars with the ends protected with an epoxy coating, three bars with the ends protected by a cap filled with epoxy, three conventional bars connected to bare conventional steel cathodes, and one bar with a reduced mortar cover.

In addition to the corrosion tests, the thickness and continuity of the stainless steel cladding is examined with a scanning electron microscope at magnifications between 11.6x and 186x. Images are taken for both transverse (through the barrel) and longitudinal (through longitudinal ribs) cutting planes.

CHAPTER 2
EXPERIMENTAL PROGRAM

This chapter describes the macrocell corrosion and corrosion potential tests used to investigate the corrosion performance of conventional and 304 stainless steel clad reinforcing bars, and the method used to evaluate the thickness and uniformity of the stainless steel cladding.

2.1 Corrosion Testing

The study consists of 46 corrosion potential and 52 macrocell corrosion tests. The test specimens and setup procedures are similar for both tests. Descriptions of the test specimen, specimen fabrication, and test procedures follow.

2.1.1 Materials

Reinforcing Steel – The reinforcing bars used in this study were manufactured by Structural Metals, Inc. (SMI). The quantity of steel consisted of 25 m (85 ft) of 304 stainless steel clad and 24 m (80 ft) of conventional No. 19 [No. 6] bars. The stainless steel clad bars were delivered in three bundles from heats as shown in Table 2.1. The chemical composition of the 304 stainless steel was not provided by SMI. Type 304 stainless steel contains between 18.0 to 20.0% chromium and 8.0 to 10.0% nickel. The conventional steel consisted of eight 10 feet long bars. The chemical composition and mechanical properties of the conventional bars were provided by SMI (Tables 2.2 and 2.3).

The clad bars were prepared as follows: First, the surface of a partial conventional steel billet was sprayed with 304 stainless steel. This partial billet was then welded to the end of a full sized conventional steel billet, and the elongated billet was hot rolled to produce the reinforcing bars. Bars were sand blasted after they were rolled

Mortar – Mortar for the rapid tests is mixed in batches consisting of 5,280 g (11.64 lbs.) of Type I portland cement, 2,640 g (5.82 lbs.) of distilled water, and 10,560 g (23.28 lbs.) of ASTM C 778 graded Ottawa sand.

The mixture has a water/cement ratio of 0.5 and a sand-cement ratio of 2.0, by weight. The mix represents the mortar constituent of concrete with a 28-day compressive strength of 28 MPa (4 ksi).

Epoxy Coating – The epoxy coating used in this study is Nap-Gard 7-2709 Rebar Patch Kit, manufactured by the Herberts O'Brien Corporation. The epoxy complies with the criteria in ASTM A 775 for repair material.

2.1.2 Test Specimen

Two types of specimens are used to evaluate the corrosion performance of the conventional and stainless steel clad reinforcing bars, a bare 127 mm (5 in.) long reinforcing bar and a specimen consisting of a 127 mm (5 in.) long bar symmetrically embedded 76 mm (3 in.) in a 38 mm (1.5 in.) or 30 mm (1.18 in.) diameter mortar cylinder (Fig. 1.3). The length of the mortar cylinder is 102 mm (4 in.).

2.1.3 Specimen Fabrication

The procedure used to fabricate bare and mortar covered test specimens is as follows:

Bar Preparation – The bars are cut with a band saw to a length of 127 mm (5 in.). One end of the bar is then drilled and tapped 13 mm (0.5 in.) to accommodate a No. 10-24 machine screw, and the edges at both ends of the bar are belt sanded to grind off any sharp edges. The bar is than soaked in acetone to remove grease, dirt, and hydraulic fluid from the surface and dried at room temperature.

For conventional steel and stainless steel clad bars that are going to be cast in mortar, electrical tape is wrapped around the entire surface area of the bar except for a 15 mm (0.6 in.) wide band centered 51 mm (2 in.) from the tapped end of the bar.

The uncovered area of the bar is then sand blasted for a minimum of 5 minutes to remove the mill scale.

For two stainless steel clad specimens (MS-7 and MS-8), the entire surface area of the bars was sandblasted. After sandblasting, the bars were cleaned in another acetone bath.

Next, two layers of epoxy are painted on the unthreaded end of the bar, or a plastic cap filled with epoxy is placed over the end. Prior to applying the second layer of epoxy or inserting the bar into the cap (partially filled with epoxy), an epoxy coating is applied over the end of the bar and allowed to cure until it becomes tacky. When a second layer of epoxy is used, it is applied a few millimeters up the sides of the bar, as shown in Fig. 1.2. When the cap is used, it is filled to about one-half of its depth with epoxy and then placed on the end of the bar. For mortar specimens, a double layer of epoxy is applied to the sandblasted part of the conventional bars and at the same location for the stainless bars. The second layer of epoxy is applied after the first layer of epoxy has cured long enough to become tacky. The epoxy is mixed and applied according to the manufacturer's directions.

Mortar Mold and Assembly – The mold is used to form a mortar cover around the reinforcing bar (Fig. 1.3). It is constructed using three sizes of PVC pipe and two rubber stoppers. It is held upright and supported by a wood frame (Fig. 2.1). The materials used to make the mold and wooden frame are listed in Table 2.4.

The assembly procedure used to place the specimen in the mold begins by inserting the tapped end of the reinforcing bar 76 mm (3 in.) through the hole of stopper D (Fig. 2.1). The bar should be inserted starting at the widest end of the stopper. Next, the bar and stopper D are placed in PVC connector E. After this is completed, stopper C is inserted into connector B until it makes contact with the shoulder on the inside surface of the connector. Connector B is then inserted into the free end of connector E. At the same time, the tapped end of the bar is pushed through the hole in stopper C. The slit along pipe G is taped closed with masking tape and then inserted into the open end of connector E. The molds are held upright

by placing them between holes cut out of the wooden boards F. Finally, the boards are clamped together with threaded rods H, securing the molds.

Mortar Mixing – The mortar is mixed following the procedures outlined in ASTM C 305.

Casting – The mortar is placed in the cylinder mold in three equal layers. Each layer is rodded 25 times using a 3.2 mm (0.125 in.) diameter rod, 305 mm (12 in.) in length. The first layer is rodded throughout its depth, making sure not to forcibly strike the bar or bottom of the mold. The succeeding layers are rodded throughout their depths, penetrating the previous layer by about 6 mm (0.25 in.). Each layer is externally vibrated for 2 minutes using a vibration table with an amplitude of 0.15 mm (0.006 in.) and a frequency of 60 Hz.

Curing – As soon as the specimens are cast and vibrated, the molds are removed from the wood frame, and covered with a moist towel and a plastic sheet for 24 hours at room temperature 72°F± 2°F (23°C±1°C). The specimens are then separated from the molds and cured in lime [$Ca(OH)_2$] saturated water (pH = 12.5) for 14 days.

On the 13^{th} day of curing, the specimens are taken out of the curing tank and placed in a plastic container filled to a depth of 115 mm (4.5 in.) with lime-saturated water. The tapped ends of the specimens are kept out of the water and air dried for 24 hours. Next, a 16 gage copper electrical wire is secured to the tapped end of each specimen with a 10-24 steel screw. The top of the screw, wire, and end of the specimen are then coated with two layers of epoxy.

2.1.4 Potential Test Procedure

The corrosion potential test measures the corrosion potential with respect to a saturated calomel electrode (SCE) for specimens exposed to a simulated concrete pore solution with a 1.6 molal ion concentration of sodium chloride (NaCl). Readings are taken daily for 40 days.

A schematic of the test configuration is shown in Fig. 1.4. The test apparatus is assembled using two plastic containers. A specimen is placed in one container and held upright by inserting it through a rectangular piece of 12.5 mm (½ in.) thick styrofoam with a length equal to the diameter of the container. The container holding the specimen is filled to a depth of 95 mm (3.72 in.) with crushed mortar fill and simulated concrete pore solution with a 1.6 molal ion concentration of NaCl. The second container is filled with saturated potassium chloride (KCl) solution, and used to hold a saturated calomel electrode (SCE). The containers are ionically connected using a salt bridge. The electrical wire on the specimen is attached to a binding post on a terminal box.

To measure corrosion potential, the positive lead of a voltmeter is plugged into the binding post on a terminal box. The negative lead of the voltmeter is connected to the SCE. The voltage reading on the voltmeter is the corrosion potential of the steel with the respect to the SCE.

The following are components used in the corrosion potential test.

Containers (with lid) – Containers are used to hold bars, mortar fill, and solutions. The container has a 3.8 liter (1 gal) capacity, and is made out of high-density polyethylene.

Salt Bridge – The salt bridge serves as an ionic pathway between the containers holding the specimen and the SCE. Each salt bridge is made using a 0.9 m (36 in.) long flexible tygon tube with an inner diameter of 6.4 mm (¼ in.) and outside diameter of 9.5 mm ($^3/_8$ in.). The tube is filled with a salt gel made from 4.5 g (0.0099 lb.) of agar, 30 g (0.0661 lb.) of potassium chloride, and 100 g (0.2205 lb.) distilled water, a quantity of ingredients adequate to make three salt bridges.

The process of making the gel consists of thoroughly mixing the agar and KCl powders. The mixture is then combined with distilled water and placed over a Bunsen burner. The three constituents are stirred over the Bunsen burner until they have the consistency of syrup. Next, the semisolid gel is poured into the tubing. The salt bridge is then put into a container of boiling water for approximately 4 hours.

The salt bridge is taken out of the boiling water and allowed to cool at room temperature. If the gel does not fully fill the tube, i.e., contains voids, the salt bridge is discarded.

The typical life span of a salt bridge is three weeks. After three weeks, the gel may liquefy and flow out of the tube. If this occurs, the test specimens must be removed from the contaminated container and cleaned with distilled water. The containers are then cleaned and filled with fresh solution. At this time, the specimens are placed back into the containers for further potential test measurements.

Simulated Concrete Pore Solution – This solution represents the liquid substance found in the saturated pores and capillaries of concrete (Farzammehr 1985). One liter of simulated concrete pore solution contains 18.81 g (0.0415 lb.) of potassium hydroxide (KOH), 17.87 g (0.0391 lb.) of sodium hydroxide (NaOH), 0.14 g (0.00031 lb.) of sodium chloride (NaCl), and 974.8 g (2.1491 lb.) of distilled water. The pH of the solution is 13.3.

The NaCl was not included in the simulated concrete pore solution in this study.

1.6 molal (m) NaCl Solution – The 1.6 m NaCl solution serves as an electrolyte. The solution is made by adding 45.6 g (0.1005 lb.) of NaCl to 1 liter (0.2642 gal) of simulated concrete pore solution.

Saturated Potassium Chloride (KCl) Solution – Saturated KCl solution is prepared by adding 500 g (1.1023 lbs.) of KCl to one liter of distilled water.

Mortar Fill – The fill acts as a buffer and simulates the relative amount of cementious material that exists in concrete structures. Mortar fill is made by filling a metal cooking sheet to a depth of 12.5 mm (1/2 in.) with the same mortar mix used for the specimens. The mortar fill is vibrated for 15 seconds on a vibration table at an amplitude of 0.15 mm (0.006 in.) and a frequency of 60 Hz. After the mortar fill has cured in air for 14 days, the mortar sheet is broken into 25 to 50 mm (1 to 2 in.) pieces.

Terminal Box – A terminal box is used to consolidate the specimen wires. The terminal box is a Radio Shack brand metal box, 178 x 102 x 50 mm (7 x 4 x 2 in.), with sixteen binding posts attached at the top.

Wire – 16 gage standard insulated copper wire is used to electrically connect the specimens to the terminal box.

Saturated Calomel Electrode – The electrode is a Fisher Scientific Brand (Catalog No. 13-620-52) saturated calomel electrode.

Voltmeter – The voltmeter is a Hewlett-Packard 3455A multi-channel digital voltmeter.

2.1.5 Potential Test Program

The corrosion potential test was performed on bare and mortar covered conventional and stainless steel clad specimens. Twelve bare conventional steel and fifteen bare stainless steel clad specimens were evaluated. Six specimens were tested with epoxy coatings over the ends of the bars, and two with the ends covered with a cap filled with epoxy. Two tests contained specimens exposed to only simulated concrete pore solution. Two more specimens were tested in a simulated concrete pore solution with air, scrubbed to remove CO_2, pumped into the solution. Three additional bare stainless steel clad specimens with a hole drilled through the cladding were tested.

Ten mortar covered conventional steel specimens in three groups and nine stainless steel clad bars in two groups were tested. For each type of bar, six tests were conducted on specimens with the ends protected by an epoxy coating, and three tests were conducted on specimens protected by a cap filled with epoxy. A single conventional steel specimen was evaluated with a reduced mortar cover to determine if a smaller cover would affect the time required for chloride ions to reach the mortar-steel interface and subsequently change the potential of the steel.

2.1.6 Macrocell Corrosion Test Procedure

The macrocell corrosion test is used to determine the corrosion rate for specimens exposed to a simulated concrete pore solution with a 1.6 molal ion concentration of NaCl. The corrosion rate is measured daily for 100 days.

A schematic of the test configuration is shown in Fig. 1.5. The testing apparatus consists of modified version of that used for the corrosion potential test. In the macrocell corrosion test, the container holding the SCE is replaced with a container holding two specimens with mortar fill and submersed in simulated concrete pore solution. The wire attached to the specimen in the first container is connected to a binding post on a terminal box. The wires from the second container are connected to a second binding post. The electrical connection is completed by placing a 10 ohm resistor between the two binding posts. A salt bridge is used to provide an ionic path between the solutions in the two containers.

To determine the macrocell corrosion rate, the voltage drop across the resistor is measured by connecting the positive lead of a voltmeter to the binding post connected to the single specimen and the negative lead to the other binding post. The voltage reading is converted to current and then current density on the surface of the reinforcing bar. The exposed surface area of one bar with the end coated with epoxy is 40.9 cm^2, and the area for a bar with the end protected with a cap is 31.9 cm^2. Faraday's law [Eq. (1.11)] is then used to calculate the macrocell corrosion rate in μm/yr.

In addition to the components needed for the corrosion potential test, the macrocell test requires:

Resistor – A 10 ohm resistor with ± 2% accuracy.

Air Scrubber – An air scrubber is used to remove carbon dioxide (CO_2) from the pressurized air that is supplied to the cathodes in the macrocell corrosion test (Fig. 1.5). Oxygen from the scrubbed air is provided to the container holding the cathodes to replenish the oxygen that is lost from the reduction reaction. The oxygen is

distributed to cathode containers through a series of interlocking air hoses. Screw adjustable hose clamps regulate the amount of air pumped into the containers.

The air scrubber consists of an 18.9 liter (5 gallon) plastic water storage container filled with a 1 molar sodium hydroxide (NaOH) solution and plastic tubing. The solution is comprised of 40 g (0.0882 lb.) NaOH per 1000 g (2.2046 lbs.) of distilled water. Air pressurized at 40-60 KPa (10-15 psi) is passed through the tubing and bubbled through the NaOH solution.

Pressurized air is pumped into the container through a hose that is inserted in a hole cut out of the top of the container. The length of the hose is long enough to coil several times at the bottom of the container. Several small holes are punctured in the coiled section of the hose to allow air to be bubbled into the NaOH solution. Another hose is inserted in a second hole at the top of the container. This hose carries the scrubbed air to the hoses that are inserted into the cathode containers of the macrocell. A high strength water-resistant plastic sealant is used to seal the interface between the hoses and the top of the container. The container is filled ¾ full of NaOH solution. Regular maintenance of the air scrubber is necessary and consists of replenishing evaporated water, adding NaOH, and resealing the interface between the hoses and container.

2.1.7 Macrocell Corrosion Test Program

The macrocell corrosion rate was measured for conventional and stainless steel clad specimens with and without a mortar cover. Nine bare conventional steel specimens in two groups and seventeen stainless steel clad specimens in five groups were tested. The first group of conventional bars consisted of six specimens with epoxy covering the untapped end of the bars. The second group consisted of three specimens with the untapped ends covered with a plastic cap filled with epoxy. The same number of stainless steel clad specimens were tested with epoxy coatings and caps as were tested in the two groups of conventional steel specimens. In the third group, the entire surface area of the stainless steel clad bars was sandblasted. The

fourth group contained three specimens with a hole drilled through the cladding to the mild steel core. The fifth group of stainless steel clad specimens consisted of three bars with holes drilled through the cladding connected to conventional steel cathodes.

Sixteen mortar covered conventional steel specimens in four groups and ten stainless steel clad specimens in three groups were tested. For each type of bar, six tests were performed on specimens with the ends protected by epoxy coatings. Six and three tests were conducted on conventional steel and stainless steel clad bars protected by a cap filled with epoxy, respectively. One conventional steel and one stainless steel clad specimen were tested with a reduced mortar cover, to determine if a smaller cover would effect the time required for chloride ions to reach the mortar-steel interface and subsequently change the corrosion rate. The fourth group of conventional steel tests contained three mortar covered specimens acting as anodes connected to bare conventional steel cathodes. The purpose of connecting the specimens to bare cathodes was to see whether the corrosion rate would be affected by the mortar surrounding the cathodes.

2.2 Scanning Electron Microscope Imaging

Sections of a stainless steel clad bar were viewed using a Philips 515 scanning electron microscope (SEM) at magnifications between 11.6x and 186x, to determine the continuity of the cladding. The thickness of the cladding was measured to the nearest 0.01 mm at 60 points around the periphery of six transverse sections. Six additional specimens showing the cladding along the longitudinal plane of the bar were evaluated.

Images were obtained using an ELMDAS digital image acquisition system. The system was configured for a pixel density of 512 x 512 and images were acquired using pixel dwell times between 131 and 915 microseconds. The SEM was operated using an accelerating voltage of 20kV and a probe diameter of 100 nm.

2.2.1 Specimen Fabrication

The specimens used to analyze the stainless steel cladding were cut from the stainless steel bar with heat number 9812048/20-8 (Table 2.1). Six transverse specimens were cut starting 50 mm (2 in.) from the end of the bar using a band saw. The first three specimens were cut side-by-side, approximately 12.7 mm (0.5 in.) in depth per specimen. The specimens were cut through the barrel of the bar. A 6.4 mm (0.25 in.) section of bar was cut after removal of the third specimen and discarded. This allowed the thickness of the next three specimens to be cut at 12.7 mm (0.5 in.) intervals through the ribs of the bar. Six more transverse specimens were cut in the same fashion as the first six. These specimens were cut a second time along the longitudinal axis of the bar. After the specimens were cut, they were cleaned in an acetone bath to remove grease, dirt, and hydraulic fluid. The faces of the specimens were then cleaned with soft soap and water. The cut surfaces were polished using, in sequential order, 150, 300, 600, and 2000 grit carborundum paper. The specimens were cleaned with soft soap and 100% ethyl alcohol between polishes. Finally, the specimens were mounted on aluminum stubs using carbon-coated tape. The specimens were placed in a humidity controlled storage container prior to viewing in the SEM.

CHAPTER 3
RESULTS AND EVALUATION

This chapter describes the corrosion potential and macrocell corrosion test results and presents an evaluation of those results. The continuity of the stainless steel cladding, based on images taken with a scanning electron microscope, and the practical and economic potential of stainless steel clad reinforcement are also discussed.

3.1 Corrosion Potential Tests

Figures 3.1 through 3.3 present the results of the corrosion potential tests using bare conventional steel specimens with the ends of the bars coated with epoxy (PB-1 – PB-6). Potentials are measured with respect to a saturated calomel electrode. Within the first week of testing, the potentials of all six specimens drop below –0.5 V, indicating a potential for rapid corrosion. After two weeks, the potentials become more positive, ranging between –0.3 to –0.45 V before returning below –0.45 to –0.5 V. The results for bare conventional bars with the ends protected with a plastic cap filled with epoxy (PBC-1 and PBC-2) are similar to those for bars PB-1 – PB-6, as shown in Fig. 3.4.

The corrosion potential test results for bare stainless steel clad specimens with the ends of the bars coated with epoxy (PS-1 – PS-6) are shown in Figs. 3.5 through 3.7. Five out of the six specimens exhibit potentials below –0.2 V (between –0.25 to –0.35 V), signifying that the bars have a tendency to corrode. A visual inspection of these bars revealed the presence of corrosion products underneath the epoxy coating at the end of the bars. The specimen that maintained a potential above –0.2 V did not show any signs of corrosion underneath the epoxy coating. Stainless steel clad specimens with the ends of the bars protected with a cap filled with epoxy (PSC-1 and PSC-2) have potentials more positive than –0.2 V, indicating that the steel is passive (Fig. 3.8). When the caps were removed from the specimens, no corrosion prod-

ucts were found. The drop in potential for the bars with the epoxy coating on the ends is likely due to crevice corrosion. Crevice corrosion occurs under the epoxy because of poor adhesion between the epoxy and steel, which leaves a narrow space between these two surfaces. This limits diffusion of dissolved oxygen from the bulk solution into the crevice. The oxygen within the small crevice is depleted, impairing passivity and increasing the concentration of metal cations. This results in the attraction of negatively charged anions such as Cl^- from the surrounding solution. The additional chloride concentration, combined with acid hydrolysis, results in a concentrated hydrochloric acid solution within the crevice, creating a localized anode coupled to a large surface area cathode on the surrounding surfaces (Jones 1996).

Two groups of corrosion potential tests were conducted on bare conventional and stainless steel specimens subjected to simulated concrete pore solution without NaCl (Figs. 3.9 – 3.12). The first group of conventional and clad specimens (PCB and PCS) exhibit nearly identical potential readings, reaching about –0.12 V at 40 days (Figs. 3.9 and 3.10), throughout the duration of the tests. The results indicate that the specimens remained passive. The second group consisted of tests with scrubbed air bubbled into the pore solution (PCBO and PCSO). The air was added to the solution to determine if the potentials would be affected by the oxygen. The results (Figs. 3.11 and 3.12) are similar to those exhibited in the first group.

The results of the tests performed on stainless steel clad bars with end caps and a hole drilled through the cladding (PSD-1 – PSD-3) are shown in Fig. 3.13. The potential of these specimens ranges between –0.15 to –0.2 V, indicating a passive corrosion state. No corrosion product was observed around the hole. The exposed mild steel core at the hole did not reduce the corrosion potentials of the specimens. The reason that the exposed mild steel did not affect the potential readings requires further study. Crevice corrosion, observed at the ends of bars protected with the epoxy coating, did not develop around the hole.

Figures 3.14 and 3.15 present the results of the corrosion potential tests using conventional steel bars embedded in mortar (PBM-1 – PBM-6). The potentials of

these specimens are highly variable, fluctuating between –0.3 and –0.6 V. The results indicate that all six of the specimens show a tendency to corrode. The potential readings for conventional steel bars embedded in mortar with the ends protected with a plastic capped filled with epoxy (PBMC-1 – PBMC-3) are shown in Fig. 3.16. The potentials of these specimens are less variable than the bars without caps, but also indicate a tendency to corrode, with values between –0.4 to –0.5 V.

The results for a potential test conducted on the conventional steel bar with the reduced thickness of mortar cover (PBMS-1) are shown in Fig. 3.17. This specimen exhibits corrosion potentials below –0.5 V.

The corrosion potential test results for stainless steel clad bars embedded in mortar (PSM-1 – PSM-6) are shown in Figs. 3.18 and 3.19. Epoxy was placed on the ends of the bars prior to casting the mortar. After two weeks, four of the specimens exhibit potentials indicating that the bars are passive (above –0.2 V). One of the other two specimens maintained a steady potential of about –0.25 V, while the other specimen remained passive for 2 weeks before gradually declining to –0.35 V. A visual inspection of the specimen with a –0.35 V potential revealed that corrosion occurred at the upper portion of the metal near the epoxy ring (Fig. 1.3). This may have occurred due to migration of the salt solution through the mortar and under the epoxy.

The results for the stainless steel clad bars embedded in mortar with the ends of the bars protected with a plastic cap filled with epoxy (PSMC-1 – PSMC-3) are shown in Fig. 3.20. All three specimens exhibit corrosion potentials between –0.2 and –0.25 V, indicating that the bars have a tendency to corrode. Inspection of these bars revealed no noticeable corrosion products on the surface or ends of the bars.

3.2 Macrocell Corrosion Tests

The macrocell corrosion rates for bare conventional steel bars with the bar ends coated with epoxy (MB-1 – MB-6) are shown in Figs. 3.21 and 3.22. The maximum corrosion rate exhibited by the specimens is just under 40 μm/yr (1.6 mils/yr), and varies between 10 and 40 μm/yr (0.4 and 1.6 mils/yr). The rates for

conventional bars with the ends protected by a cap filled with epoxy (MBC-1 – MBC-3) are similar, fluctuating between 15 and 35 μm/yr (0.6 and 1.4 mils/yr) (Fig. 3.23).

The corrosion rates for the bare stainless steel clad bars with the bar ends coated with epoxy (MS-1 – MS-6), shown in Figs. 3.24 and 3.25, exhibit more variation than do those for the bare conventional steel specimens. The corrosion rates for specimens MS-3 (Fig. 3.24) and MS-6 (Fig 3.25) [1.5 to 0.5 μm/yr (0.06 to 0.02 mils/yr)] are on the order of $^1/_{10}$ to $^1/_{80}$ of the rate exhibited by the bare conventional steel bars. The corrosion rates of the remaining four specimens are between 15 to 35 μm/yr (0.6 to 1.4 mils/yr), values that are similar to values observed for the conventional specimens. The high corrosion rates for the stainless steel clad specimens may be attributed to crevice corrosion. In contrast to the stainless steel specimens with epoxy coatings, all of the bars with end caps (MSC-1 – MSC-3) have corrosion rates between 0.0 to 0.3 μm/yr (0 to 0.01 mils/yr), as shown in Fig. 3.26, averaging about $^1/_{100}$ of the value observed for conventional specimens.

Sandblasted stainless steel clad specimens with ends coated with epoxy (MS-7 and MS-8) have results that are similar to those of specimens MS-1 through MS-6. The corrosion rate of MS-7 remains about 1.5 μm/yr (0.06 mils/yr) throughout the test, while MS-8 has a corrosion rate that varies between 5 and 20 μm/yr (0.2 and 0.8 mils/yr) (Fig. 3.27).

The corrosion rates for stainless steel clad bars with end caps and a hole drilled through the cladding are shown in Figs. 3.38 and 3.39. The specimens were tested using two configurations. The first configuration consists of "damaged" bars connected to stainless steel cathodes (MSD-1 – MSD-3) (Fig. 3.28), and the second configuration uses damaged bars combined with conventional steel cathodes (MSDB-1 – MSDB-3) (Fig. 3.29). For both test configurations, the corrosion rates vary between 0.0 to 0.75 μm/yr (0.0 to 0.03 mils/yr), approximately $^1/_{50}$ of the value exhibited the conventional bars. No visible corrosion was present on the damaged stainless steel clad bars.

Figures 3.30 through 3.33 present the results of the macrocell corrosion tests using conventional steel bars encased in mortar. The macrocell corrosion rate of bars with ends coated with epoxy (MBM-1 – MBM-9) varies between 2 and 5 μm/yr (0.08 and 0.2 mils/yr) (Fig. 3.30 – 3.32). These values are considerably lower than the 10 to 40 μm/yr (0.4 to 1.6 mils/yr) rates for bare conventional steel specimens. The 2 to 5 μm/yr (0.08 and 0.2 mils/yr) rates match the macrocell corrosion rates obtained in earlier research using conventional steel specimens embedded in mortar (Schwensen, Darwin, and Locke 1995, Senecal, Darwin, and Locke 1995). The macrocell corrosion rates of mortar covered bars with the ends protected by a plastic cap filled with epoxy (MBMC-1 – MBMC-3) are shown in Fig. 3.33. Two of the specimens exhibit rates between 0.5 to 2 μm/yr (0.02 to 0.08 mils/yr), while the third specimen has a rate of only 0.25 μm/yr (0.01 mils/yr).

The corrosion rates of conventional steel bars embedded in mortar combined with bare conventional steel cathodes (MM-1 – MM-3) vary between 1.0 and 5 μm/yr (0.04 and 0.2 mils/yr) (Fig. 3.34).

The results for stainless steel clad bars embedded in mortar are shown in Figs. 3.35 through 3.37. The corrosion rates of bars with ends protected by epoxy (MSM-1 – MSM-3) and plastic caps filled with epoxy (MSMC-1 – MSMC-3) range between 0.0 to 0.2 μm/yr (0.0 to 0.008 mils/yr), $^{1}/_{20}$ to $^{1}/_{50}$ of the value exhibited by the conventional bars embedded in mortar. The epoxy coatings over the ends of the stainless bars remained intact, and no crevice corrosion was observed.

A comparison of corrosion rates between conventional and stainless steel clad bars embedded in mortar with a reduced cover is shown in Fig. 3.38. The corrosion rate of the stainless steel specimen varies between 0.0 and 0.2 μm/yr (0.0 and 0.008 mils/yr), while the rate of the conventional specimen fluctuates between 0.5 to 5 μm/yr (0.02 to 0.2 mils/yr).

3.3 Cladding Thickness

Images of the stainless steel cladding obtained with the scanning electron microscope are shown in Figs. 3.39 through 3.49. Figs. 3.39 through 3.40 are images of longitudinal sections cut through transverse ribs of a stainless steel bar. The images show that, although the thickness of the stainless steel cladding varies, the cladding exhibits no breaks. Figs. 3.41 through 3.49 show images of transverse sections cut through the barrel of a stainless steel bar. As shown in Table 3.1, the thickness of the cladding varies between 0.196 mm and 0.894 mm (7.7 and 35 mils). The thickest part of the cladding is observed near an indentation in the core material, which is located along the side of a longitudinal rib, as shown in Fig. 3.46. The indentation penetrates the core to a depth of about 1.8 to 2 mm (71 to 79 mils). A 1.0 to 1.4 mm (39 to 55 mil) long crack exists in the center of the indent. The crack, however, does not penetrate the cladding. Another 1.5 μm (0.06 mil) crack (Figs. 3.48 and 3.49) is observed near the indention between the cladding and conventional steel. The thinnest part of the cladding is located on the barrel of the bar.

3.4 Practical Considerations

Considering an average corrosion rate of about 0.2 μm/yr (0.008 mils/yr) for the stainless bars, the cladding thickness appears to be satisfactory if the current minimum thickness of 0.196 mm (7.7 mils) on the prototype is maintained in production. Although the stainless clad bars show superior corrosion resistance compared to the conventional steel bars, the presence of an indention in the cladding and its associated crack may present problems if not corrected in full-scale production.

The short-term tests used in this study are meant to provide a preliminary evaluation of a corrosion protection system. Therefore, longer term tests, Southern Exposure and cracked beam tests, are recommended to more fully evaluate the new bars. Additional tests should include combinations of 304 stainless steel clad bars and conventional steel to evaluate potential drawbacks, such as observed by McDonald, Pfeifer, and Sherman (1998), indicating that the corrosion performance of solid

304 stainless steel reinforcing bars decreases when combined with conventional reinforcing steel. Other stainless steel cladding, such as type 316, should also be evaluated.

The small number of bars tested with holes in the cladding exhibited little corrosion, in contrast to the high corrosion rates observed when epoxy coating was used to protect the cut ends of the bars. This suggests a significant difference in the nature of corrosion that occurs on a fully-exposed surface as opposed to one that is subject to crevice corrosion, such as the epoxy-coated ends. Thus, although caps filled with epoxy or other techniques to seal the ends of the bars are recommended, with additional study it may be possible to allow unprotected ends.

Based on an earlier description of the results presented in this report (Darwin, Locke, Balma, and Kahrs 1999), Kepler, Darwin, and Locke (2000) compared stainless steel clad reinforcement with other corrosion protection systems. Using 1999 costs, they found that stainless steel clad reinforcement provided the lowest present value cost of all of the systems evaluated. The low cost resulted from the relatively low cost of the reinforcement and the expectation that no repair or maintenance would be required during the 75-year economic life used for the comparisons. The analysis by Kepler et al. (2000) was based on a cost of \$1.76/kg for stainless steel clad reinforcement compared to \$1.30/kg for conventional reinforcement, \$1.45/kg for epoxy-coated reinforcement, and \$1.63/kg for galvanized reinforcement. More recent discussions with Structural Metals, Inc., the company planning to produce this steel, indicates that the cost of the stainless steel clad reinforcement will increase by \$0.95/kg, producing an in-place cost of \$2.71/kg. Based on an average reinforcement quantity of 32.7 kg/m^2 for Kansas bridge decks, the initial cost of construction for a 230 mm deck (with other costs for deck construction totaling \$97/m^2) are \$186/m^2 for stainless steel clad reinforcement, \$140/m^2 for conventional reinforcement, \$144/m^2 for epoxy-coated reinforcement, and \$150/m^2 for galvanized reinforcement. Of the four methods of construction, only the stainless steel clad reinforcement will not require repair during a 75-year period. Kepler et al. estimated that a bridge deck con-

taining conventional bars with no protection would require repairs at 25 and 50 years, a bridge deck with epoxy-coated steel would require repairs at 30 and 55 years, and a bridge deck with galvanized reinforcement would require repairs at 27 and 52 years. Based on 1999 dollars, the repair cost in all cases was calculated to be $\$259/m^2$. With the exception of stainless steel clad reinforcement, the present value of the total cost depends upon the discount rate; the discount rate does not affect the present value cost of stainless steel clad reinforcement because the total cost equals the initial construction cost. For a discount rate of 2% (close to the value used by the State of Kansas), the present value of all costs for a 75-year economic life is $\$186/m^2$ for stainless steel clad reinforcement, $\$379/m^2$ for conventional reinforcement, $\$365/m^2$ for epoxy-coated reinforcement, and $\$395/m^2$ for galvanized reinforcement. At 4%, these values are, respectively, $\$186/m^2$, $\$259/m^2$, $\$245/m^2$, and $\$275/m^2$. At 6%, the costs are $\$186/m^2$, $\$199/m^2$, $\$191/m^2$, and $\$216/m^2$.

It is clear from this economic comparison that stainless steel clad reinforcing bars offer significant economic advantages over the other forms of steel reinforcement. This advantage is further strengthened when the intangible cost savings to the traveling public are considered. Therefore, although the steel has not been fully evaluated in long-term tests, stainless steel clad reinforcement of the type evaluated in this study deserves careful consideration for implementation in new bridge deck construction and should be accepted for use on a trial basis at the earliest possible date.

CHAPTER 4
SUMMARY AND CONCLUSIONS

4.1 Summary

The corrosion performance of type 304 stainless steel clad bars is compared to that of conventional steel reinforcement. The steel bars are evaluated using rapid corrosion potential and macrocell corrosion tests developed at the University of Kansas. Corrosion potential and macrocell corrosion rates are measured. In addition to the rapid corrosion tests, the thickness and uniformity of the stainless steel cladding is examined using a scanning electron microscope.

The corrosion potential and macrocell corrosion tests are conducted on bare bars and bars embedded in mortar. A water/cement ratio of 0.5 and a sand/cement ratio of 2 is used for all mortar specimens. The corrosive environment used to evaluate the corrosion performance of the steels is simulated concrete pore solution with a 1.6 molal ion concentration of sodium chloride. Corrosion potential tests include: bars with ends protected with epoxy and with plastic caps filled with epoxy, stainless steel bars with a hole drilled through the cladding, specimens with a reduced thickness of mortar cover, and specimens subjected to simulated pore solution, with and without an external supply of oxygen to the solution. Macrocell corrosion tests include: bars with ends protected with epoxy and with plastic caps filled with epoxy, stainless steel bars with a hole drilled through the cladding, stainless steel bars with a hole drilled through the cladding connected to conventional steel cathodes, specimens with a reduced thickness of mortar cover, stainless steel specimens with the surface of the bars sandblasted, and mortar covered conventional steel specimens connected to bare conventional cathodes.

The thickness of the stainless steel cladding is measured at 60 points around the periphery of the bars on transverse sections. Longitudinal sections are also examined.

4.2 Observations and Conclusions

The following observations and conclusions are based on the test results presented in this report.

1. The results of the corrosion potential and macrocell corrosion tests indicate that 304 stainless steel clad bars have significant chloride corrosion resistance, making the reinforcement a good candidate for use in concrete structures subjected to deicers and marine environments.
2. Stainless steel clad bars not encased in mortar exhibit macrocell corrosion rates between 0.0 to 0.3 μm/yr (0.0 to 0.012 mils/yr), averaging about $^{1}/_{100}$ of the value observed for conventional bars.
3. Mortar covered stainless steel bars show corrosion rates between 0.0 and 0.2 μm/yr (0.0 and 0.008 mils/yr), averaging $^{1}/_{20}$ to $^{1}/_{50}$ of the value exhibited by conventional bars embedded in mortar.
4. The bare clad bars with a drilled hole through the cladding corrode at rates between 0.0 to 0.75 μm/yr (0.0 to 0.03 mils/yr), averaging about $^{1}/_{70}$ of the value observed for conventional bars. The corrosion potential of the bars indicate that they are in a passive condition.
5. If the cut ends of stainless steel clad bars are coated with epoxy only, the macrocell corrosion rate is approximately the same as for conventional steel bars. Thus, caps filled with epoxy or other techniques that seal the ends of bars should be used to protect the ends of all bars. Epoxy coatings applied to the ends of bars will not provide protection.
6. The stainless steel cladding thickness varies between 0.196 to 0.894 mm (7.7 to 35 mils) around the periphery of the bar. Imperfections in the form of an indentation in the base material and a crack in the cladding material filling the indention were observed. The crack did not penetrate the stainless steel cladding, and the cladding is of adequate thickness to protect the mild steel core.

4.3 Implementation Plan

Based on the tests performed in this study, stainless steel clad reinforcing bars provide significantly improved corrosion performance compared to conventional steel, and even epoxy-coated reinforcement, the principal corrosion protection system in use today. While additional tests are required to answer a number of remaining questions involving this form of reinforcement, the advantages demonstrated in this study indicate that the steel should be accepted for use on a trial basis. Therefore, it is recommended that stainless steel clad reinforcement serve as one of the corrosion protection systems to be used in a planned series of demonstration decks under the current KDOT contract.

4.4 Recommendations for Future Study

1. Further testing should be conducted on the stainless steel clad bars, including the Southern Exposure and cracked beam tests. The Southern Exposure and cracked beam tests are longer-term tests, that are used to realistically simulate the formation of corrosion macrocells in reinforced concrete structures.
2. Corrosion tests should be performed using 304 stainless steel clad anodes combined with conventional steel cathodes. A previous study (McDonald, Pfeifer, and Sherman 1998) has indicated that the corrosion performance of 304 stainless steel decreases when a macrocell develops between 304 stainless steel and conventional steel.
3. Other types of stainless steels, such as type 316, should be evaluated as a cladding material.
4. Mechanical and fatigue testing should be conducted on the stainless steel clad bars, along with inspection of the fatigued cladding.
5. Considering the small number of tests on bars with holes through the cladding, additional tests should be conducted to determine the effects of

damaged cladding and unprotected ends on the corrosion performance of the bars.

REFERENCES

ACI Committee 222, (2001). "Corrosion of Metals in Concrete ACI 222R-96," *ACI Manual of Concrete Practice*, Part 1, American Concrete Institute, Farmington Hills, MI.

ASTM C 305-99, (2000). "Standard Practice for Mechanical Mixing of Hydraulic Cement Pastes and Mortars of Plastic Consistency," *2000 Annual Book of ASTM Standards*, Vol. 4.01, American Society for Testing and Materials, West Conshohocken, PA.

ASTM A 775/A 775M-00b, (2001). "Standard Specification for Epoxy-Coated Reinforcing Steel Bars," *2001 Annual Book of ASTM Standards*, Vol. 1.04, American Society for Testing and Materials, West Conshohocken, PA.

ASTM C 778-00, (2001). "Standard Specification for Standard Sand," *2001 Annual Book of ASTM Standards*, Vol. 4.01, American Society for Testing and Materials, West Conshohocken, PA.

ASTM C 876-91, (2001). "Standard Test Method for Half-Cell Potentials of Uncoated Reinforcing Steel in Concrete," 2000 *Annual Book of ASTM Standards*, Vol. 4.02, American Society of Testing and Materials, West Conshohocken, PA.

Beddoes, J., Parr, G. J., (1999). *Stainless Steels*, 3rd Ed., ASM International, Materials Park, OH.

Broomfield, J. P., Rodriguez, J., Ortega, L. M., and Garcia, A. M., (1993). "Corrosion Rate Measurement and Life Prediction for Reinforced Concrete Structures," *Proceedings of the Structural Faults and Repair*-93, University of Edinburgh, Scotland, Vol. 2, pp. 155-164.

Clear, K.C., (1989). "Measuring Rate of Corrosion of Steel in Field Concrete Structures," *Transportation Research Record* 1211 (Washington, D.C.: Transportation Research Board), pp. 28-37.

Darwin, D., Locke, C. E, Jr., Balma, J., and, Kahrs, J. T., (1999). "Evaluation of Stainless Steel Clad Reinforcing Bars," *SL Report* 99-3, University of Kansas Center for Research, Lawrence, KS, 17 pp.

Farzammehr, H., (1985). "Pore Solution Analysis of Sodium Chloride and Calcium Chloride Containing Cement Pastes," *Master of Science Thesis*, University of Oklahoma, Norman, OK.

Jones, D. A., (1996). *Principles and Prevention of Corrosion*, 2nd Ed., Prentice-Hall, Inc., Upper Saddle River, NJ.

Kepler, J. L., Darwin, D., and Locke, C. E., (2000). "Evaluation of Corrosion Protection Methods for Reinforced Concrete Highway Structures," *SM Report* No. 58, University of Kansas Center for Research, Lawrence, KS, 221 pp.

Larkin, A. G., (1966). "Stainless Steel – Its Origin," *Metallurgia*, Vol. 73, No. 438, April, pp. 165-166.

Martinez, S. L., Darwin, D., McCabe, S. L., and Locke, C. E., Jr., (1990). "Rapid Test for Corrosion Effects of Deicing Chemicals in Reinforced Concrete," *SL Report* 90-4, University of Kansas Center for Research, Lawrence, KS, 61 pp.

Maurer, E., (1933). "Zur Entstehung Der Rosticheren Stahle," *Ztschr. Elektrochem.*, Vol. 39, No. 10, pp. 820-824.

McDonald, D. B., Sherman, M. R., Pfeifer, D. W., and Virmani, Y. P., (1995). "Stainless Steel Reinforcing as Corrosion Protection," *Concrete International*, Vol. 17, No. 5, May, pp. 65-70.

McDonald, D. B., Pfeifer, D. W., and Blake, G. T., (1996). "The Corrosion Performance of Inorganic-, Ceramic-, and Metallic-Clad Reinforcing Bars and Solid Metallic Reinforcing Bars in Accelerated Screening Tests," *Report* No. FHWA-RD-96-085, Federal Highway Administration, Office of Engineering and Highway Operations R&D, McLean, VA, Oct., 112 pp.

McDonald, D. B., Pfeifer, D. W., and Sherman, M. R., (1998). "Corrosion Evaluation of Epoxy-Coated, Metallic-Clad and Solid Metallic Reinforcing Bars in Concrete," *Publication* No. FHWA-RD-98-153, Federal Highway Administration, McLean, VA, Dec., 127 pp.

Monnartz, P., (1911). "Beitrag Zum Studium Der Eisenchromlegierungen," *Metallurgie*, Vol. 8, No. 1, pp. 161-193.

National Research Council (U.S.), Committee on the Comparative Costs of Rock Salts and Calcium Magnesium Acetate (CMA), (1991). "Highway Deicing-Comparing Salt and Calcium Magnesium Acetate," *Special Report* 235, Transportation Research Board, Washington, DC, pp. 170.

Page, C. L., and Treadway, K. W. J., (1992). "Aspects of the Electrochemistry of Steel in Concrete," *Nature*, Vol. 297, No. 5862, May, pp. 109-115.

Rasheeduzzafar A., Dakhil F. H., Bader, M. A., and Khan, M. M., (1992). "Performance of Corrosion Resisting Steel in Chloride Bearing Concrete," *ACI Materials Journal*, Vol. 89, Sep. - Oct., pp. 439-448.

Revie, Winston, R., (2000). *Uhlig's Corrosion Handbook*, 2nd Ed., John Wiley & Sons Inc., New York.

Schiessl, P., (1988). "Corrosion of Steel in Concrete," *Report of the Technical Committee* 60-CSC, RILEM, Chapman and Hall, New York, 97 pp.

Schwensen, S. M., Darwin, D., and Locke, C. E., Jr., (1995). "Rapid Evaluation of Corrosion-Resistant Concrete Reinforcing Steel in the Presence of Deicers," *SL Report* 95-6, University of Kansas Center for Research, Inc., Lawrence, KS, 90 pp.

Sedriks, John, A., (1996). *Corrosion of Stainless Steels*, 2nd Ed., John Wiley & Sons Inc., New York.

Senecal, M. R., Darwin, D., and Locke, C. E., Jr., (1995). "Evaluation of Corrosion-Resistant Steel Reinforcing Bars," *SM Report* No. 40, University of Kansas Center for Research, Inc., Lawrence, KS, 142 pp.

Sorensen, B., Jensen, P. B., and Maahn, E., (1990). "The Corrosion Properties of Stainless Steel Reinforcement," *Corrosion of Reinforcement in Concrete,* C. L., Page, K W. J. Treadaway and P. B. Bamforth, eds., Elsevier, Applied Science, New York.

Stearn, M. S., and Geary, A. J., (1957). "Electrochemical Polarization," *Journal of the Electrochemical Society*, Vol. 104, No. 1, Jan., pp. 56-63.

Stearn, M. S., and Weisert, E. D., (1959). "Experimental Observations on the Relation Between Polarization Resistance and Corrosion Rate," *Proceedings of the ASTM*, Vol. 59, pp. 1280-1284.

Stearn, M. S., and Geary, A. J., (1958). "The Mechanism of Passivating-Type Inhibitors," *Journal of the Electrochemical Society*, Vol. 105, No. 11, pp. 638-647.

Zoob, A. B., Le Claire, P. J., and Pfeifer, D. W., (1985). *Corrosion Protection Tests on Reinforced Concrete With Solid Stainless Steel Reinforcing Bars for Joslyn Stainless Steels*, Wiss, Janney, Elstner Associates, Inc., Report.

TABLES

Table 1.1 – Standard Reference Electrodes (Jones 1996)

Name	Half-Cell Reaction	Potential (V) versus SHE
Mercury-Mercurous Sulfate	$HgSO_4 + 2e^- \rightleftarrows Hg + SO_4^{2-}$	+0.615
Copper-Copper Sulfate	$CuSO_4 + 2e^- \rightleftarrows Cu + SO_4^{2-}$	+0.318
Saturated Calomel	$HgCl_2 + 2e^- \rightleftarrows 2Hg + 2Cl^-$	+0.241
Silver-Silver Chloride	$AgCl + e^- \rightleftarrows Ag + Cl^-$	+0.222
Standard Hydrogen	$2H^+ + 2e^- \rightleftarrows H_2$	+0.000

Table 2.1 – Identification of stainless steel clad bars

Heat No.	Name	Length
1	9812048/20-8	4 bars @ 3 m (10 ft) each
2	9812036/10-5	4 bars @ 3 m (10 ft) each
3	9812050/24-9	1 bar @ 1.5 m (5 ft)

Table 2.2 – Chemical composition of conventional bars

Composition (%)							
Cr	**Ni**	**C**	**Mn**	**Si**	**P**	**S**	**Other**
0.19	0.24	0.4	0.89	0.022	0.01	0.022	Cu 0.47, Mo 0.058, V 0.003, Sn 0.014

Table 2.3 – Mechanical properties of conventional steel

Tensile Strength (MPa)	Yield Strength (0.2% Offset) (MPa)	Elongation (%)
739	469	13.5

Table 2.4 – Materials used to fabricate molds for eight specimens

Label	No.	Description
A	2	38 x 286 mm (nominal 2 x 12 in.) CCA treated lumber
B	8	58 x 60 mm (2.3 x 2.36 in.) PVC fitting
C	8	No. 9 laboratory grade rubber stopper with a 17 mm (0.625 in.) diam. hole through the center
D	8	No. 6.5 laboratory grade rubber stopper with a 17 mm (0.625 in.) diam. hole through the center
E	8	50 x 66 mm (2 x 2.60 in.) PVC fitting
G	8	102 x 42 mm (4 x 1.65 in.) PVC fitting
H	6	6 x 305 mm (0.25 x 12 in.) No. 10-40 threaded screw

Table 3.1 – Variation in cladding thickness for transversely cut specimens

Specimen	Minimum (mm)	Maximum (mm)	Mean (mm)
1	0.196	0.844	0.488
2	0.301	0.894	0.524
3	0.226	0.864	0.453
4	0.245	0.750	0.445
5	0.243	0.726	0.442
6	0.255	0.735	0.450
Total	0.196	0.894	0.467

1 mm = 0.0394 in. = 39.4 mils

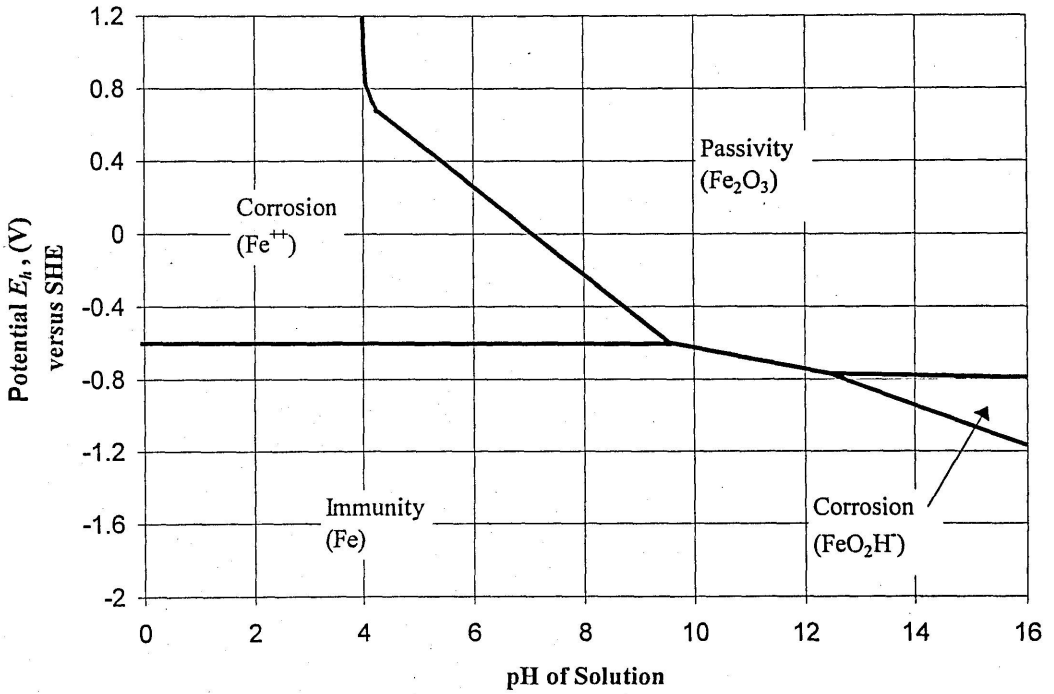

Fig. 1.1 – Simplified Pourbaix diagram showing the domains of corrosion behavior for the Fe-H_20 system at 25 °C (77 °F) (Beddoes and Parr 1999).

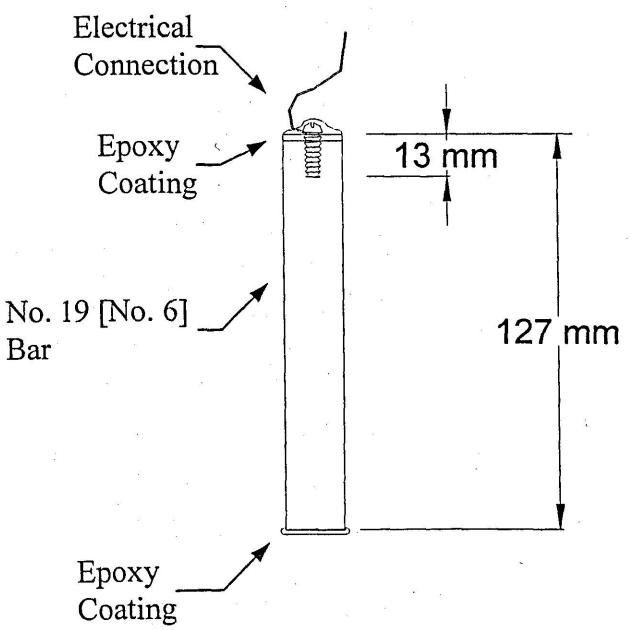

Figure 1.2 – Cross-Section of Bare Specimen

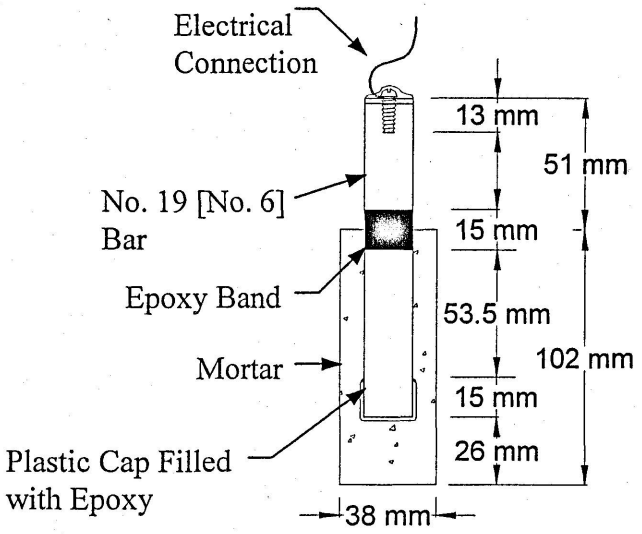

Figure 1.3 – Cross-Section of Mortar Specimen

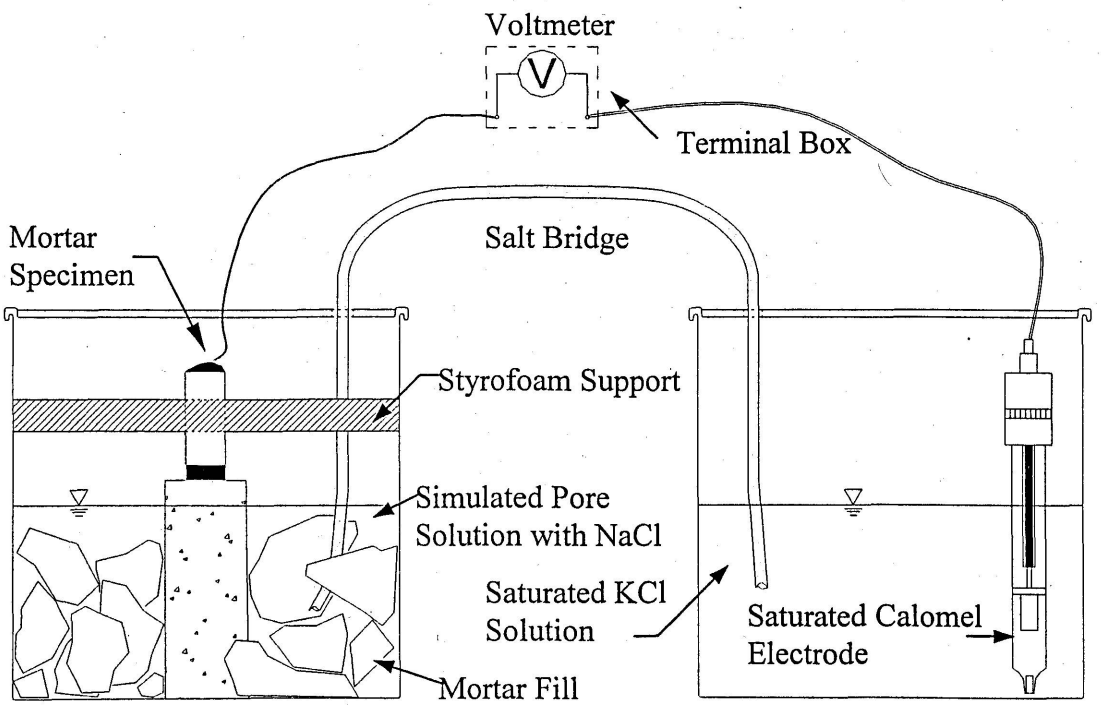

Figure 1.4 – Schematic of Corrosion Potential Test

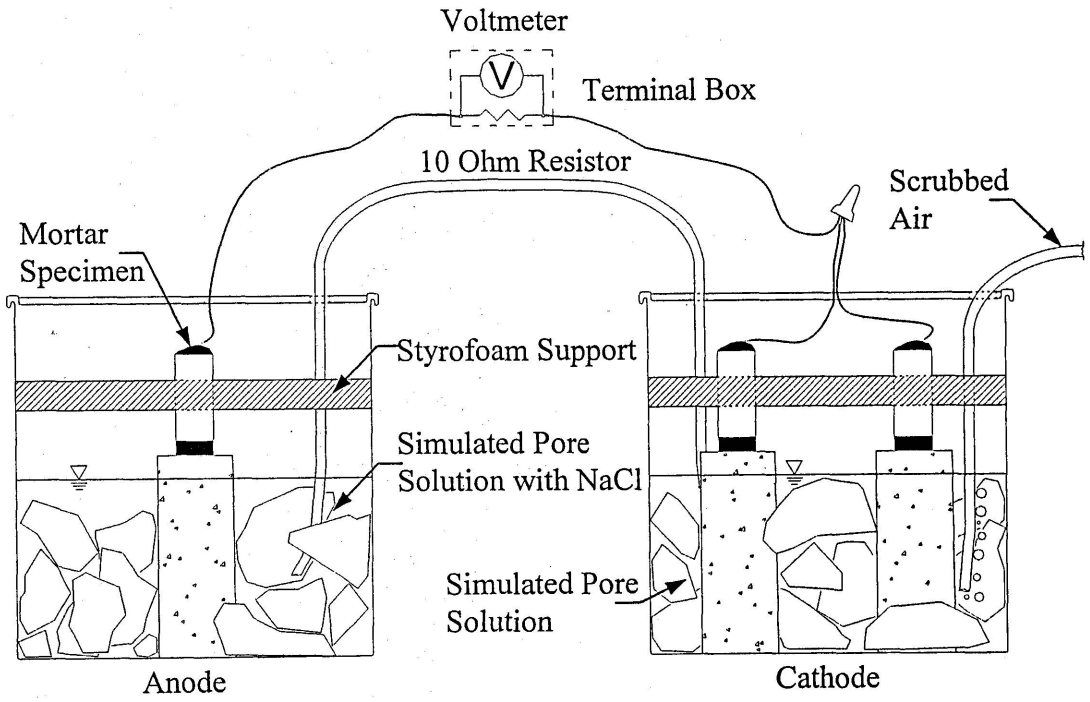

Figure 1.5 – Schematic of Macrocell Corrosion Test

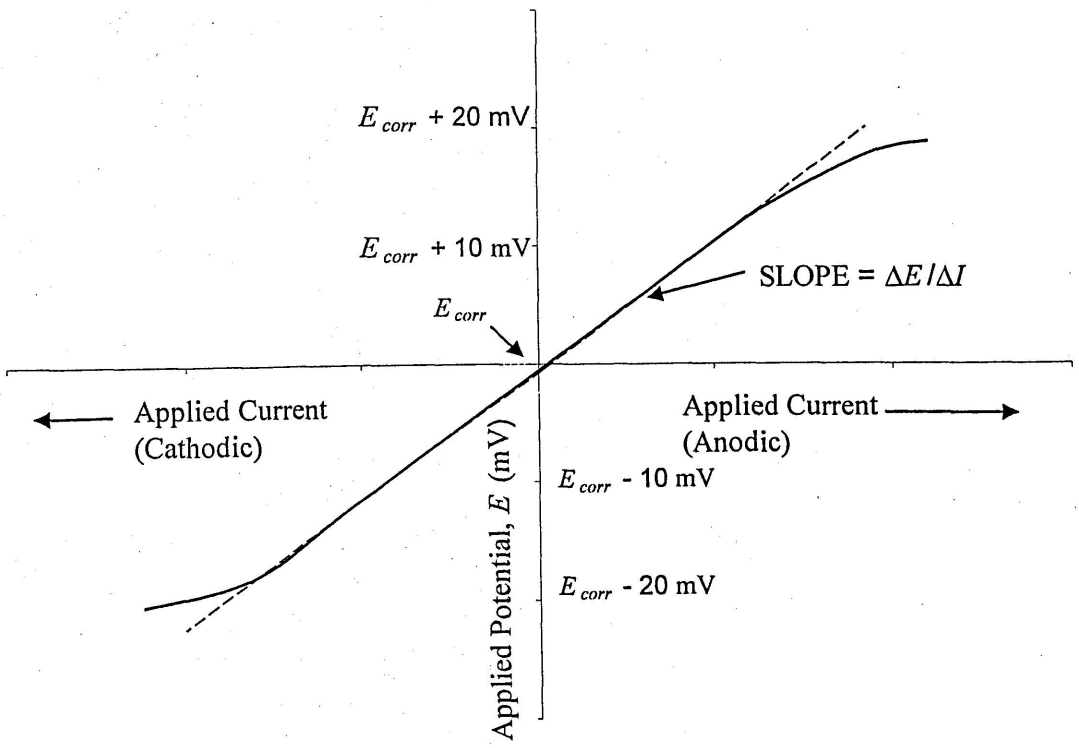

Figure 1.6 – Linear Polarization Curve (Sedriks 1996)

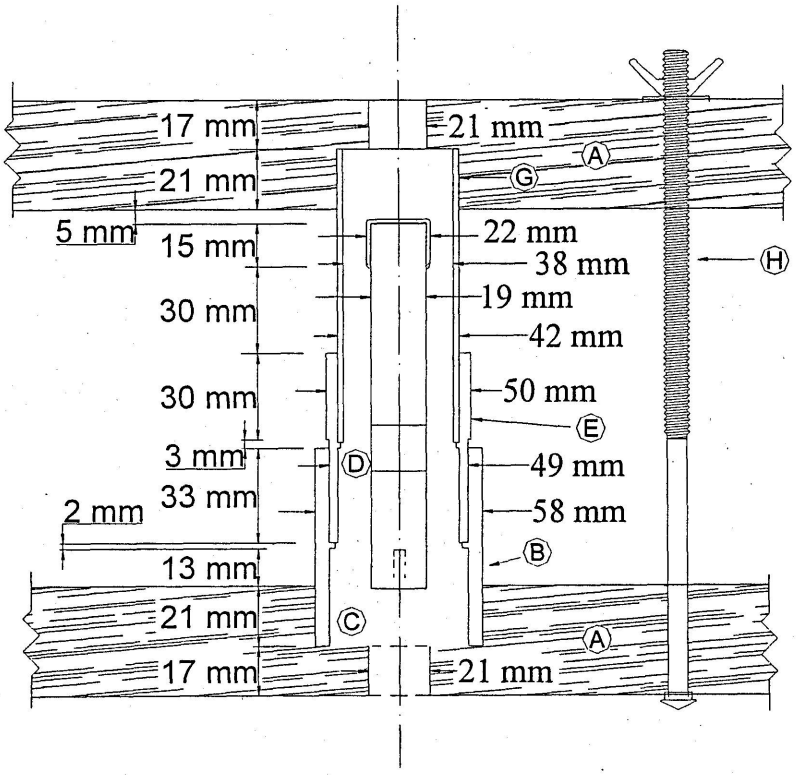

Figure 2.1 – Cross-Section of Specimen Mold

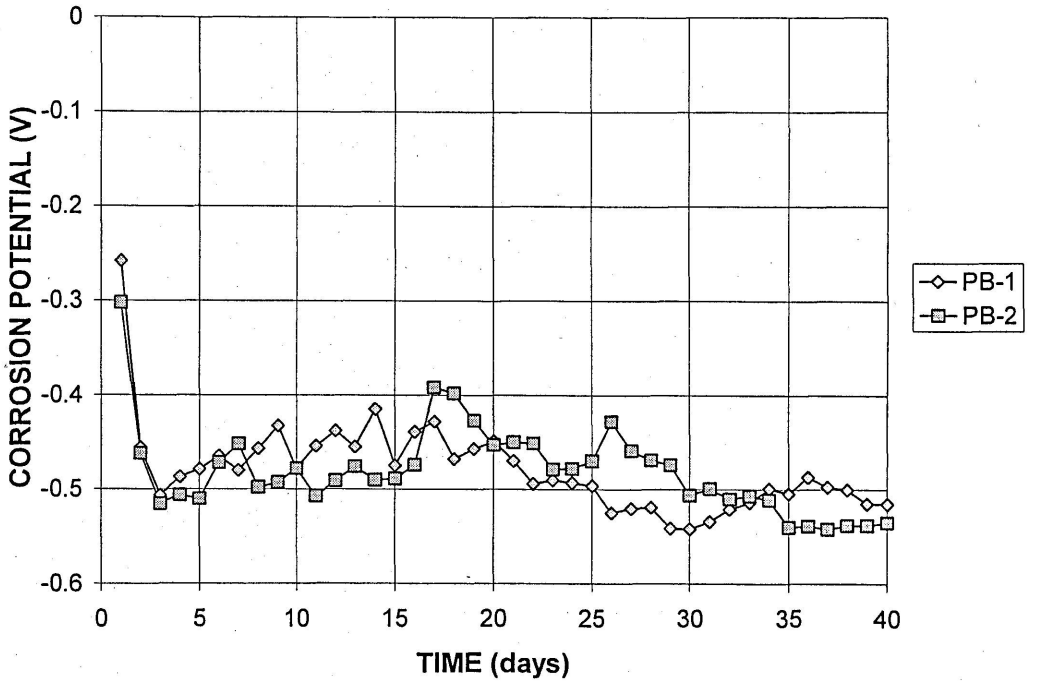

Figure 3.1 – Corrosion potential versus time for bare conventional steel bars with epoxy on the ends and exposed to 1.6 m NaCl in simulated pore solution: Specimens PB-1 and PB-2

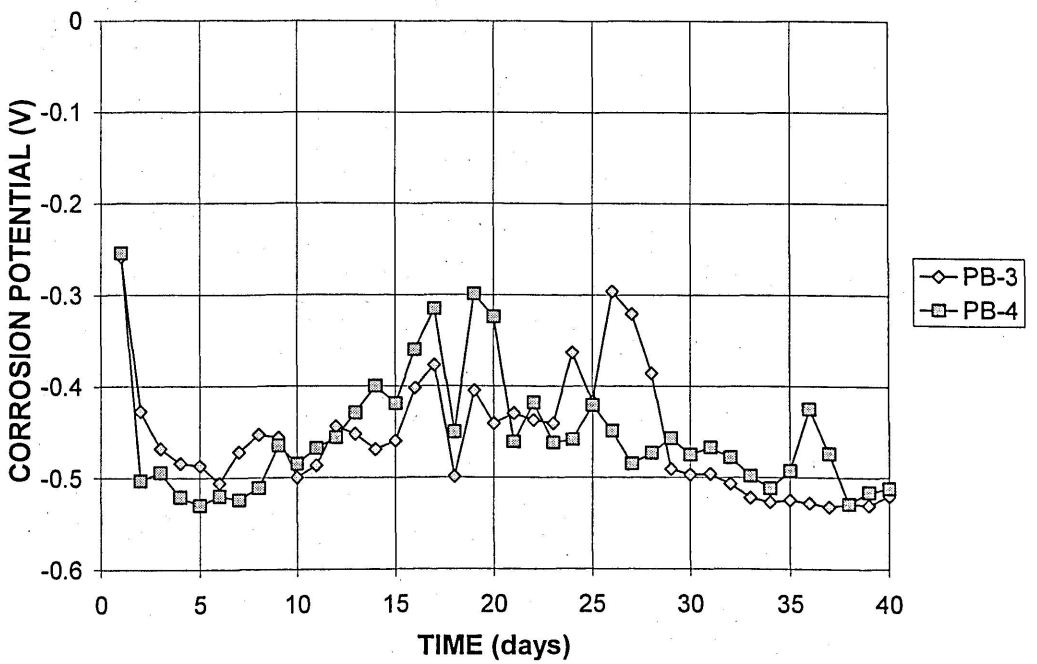

Figure 3.2 – Corrosion potential versus time for bare conventional steel bars with epoxy on the ends and exposed to 1.6 m NaCl in simulated pore solution: Specimens PB-3 and PB-4

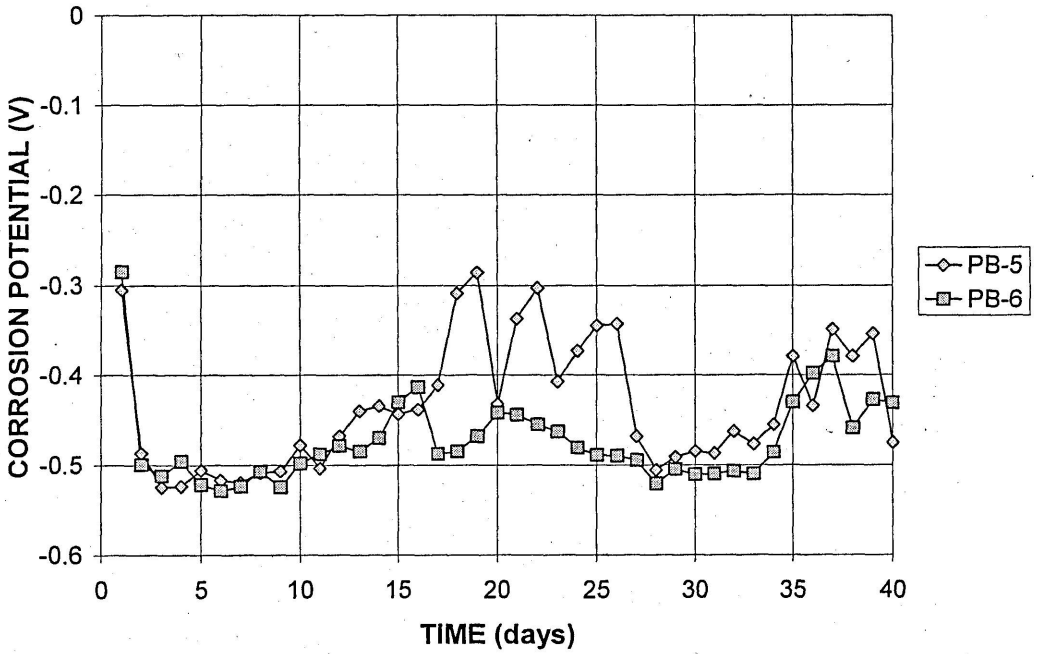

Figure 3.3 – Corrosion potential versus time for bare conventional steel bars with epoxy on the ends and exposed to 1.6 m NaCl in simulated pore solution: Specimens PB-5 and PB-6

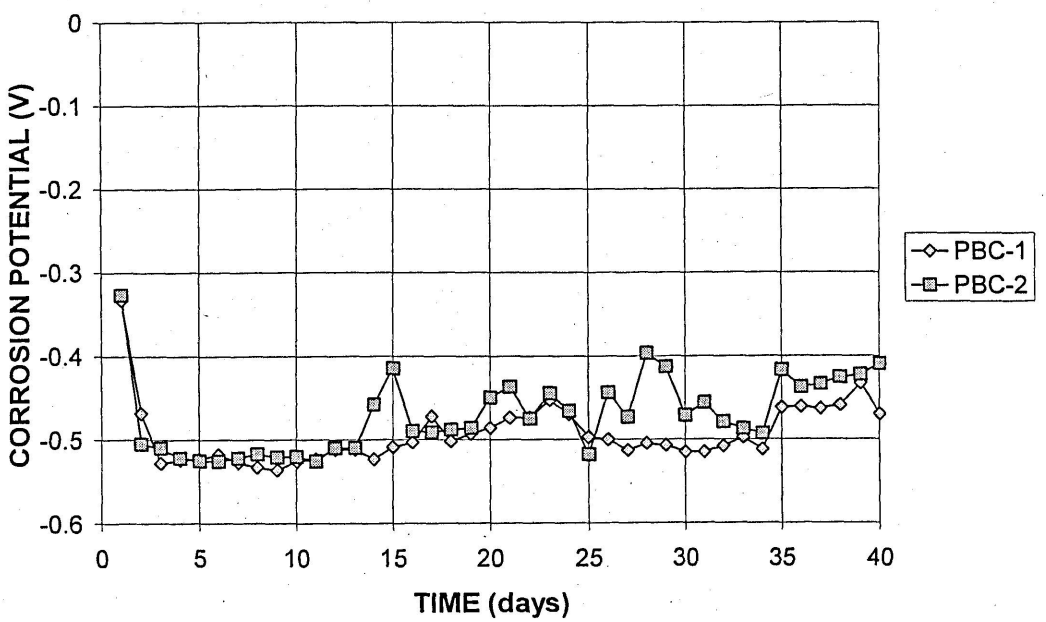

Figure 3.4 – Corrosion potential versus time for bare conventional steel bars with caps exposed to 1.6 m NaCl in simulated pore solution: Specimens PBC-1 and PBC-2

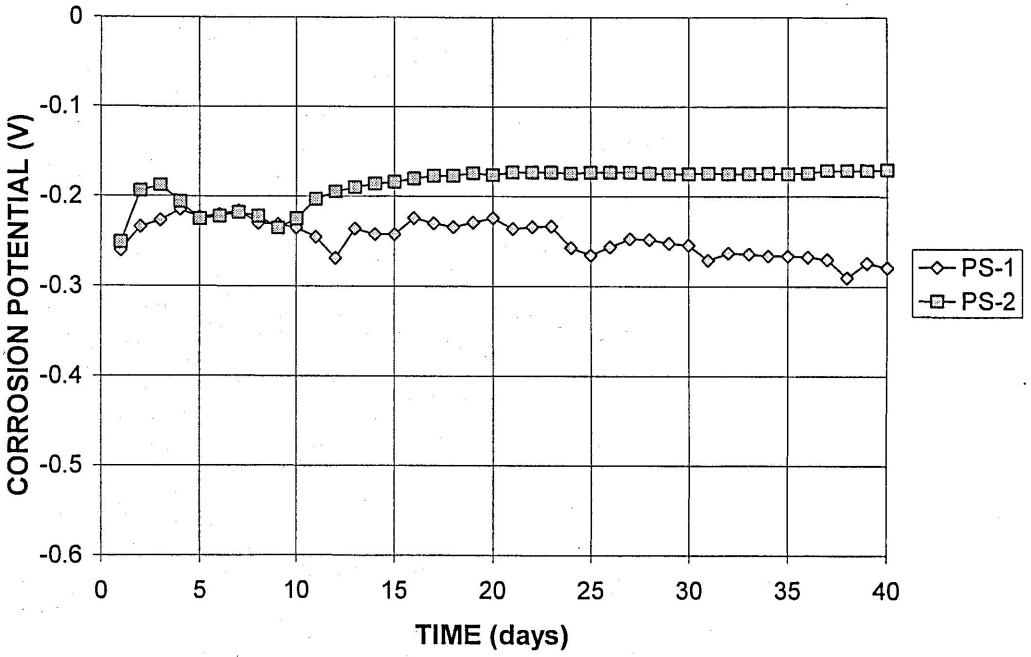

Figure 3.5 – Corrosion potential versus time for bare stainless steel clad bars with epoxy on the ends and exposed to 1.6 m NaCl in simulated pore solution: Specimens PS-1, PS-2

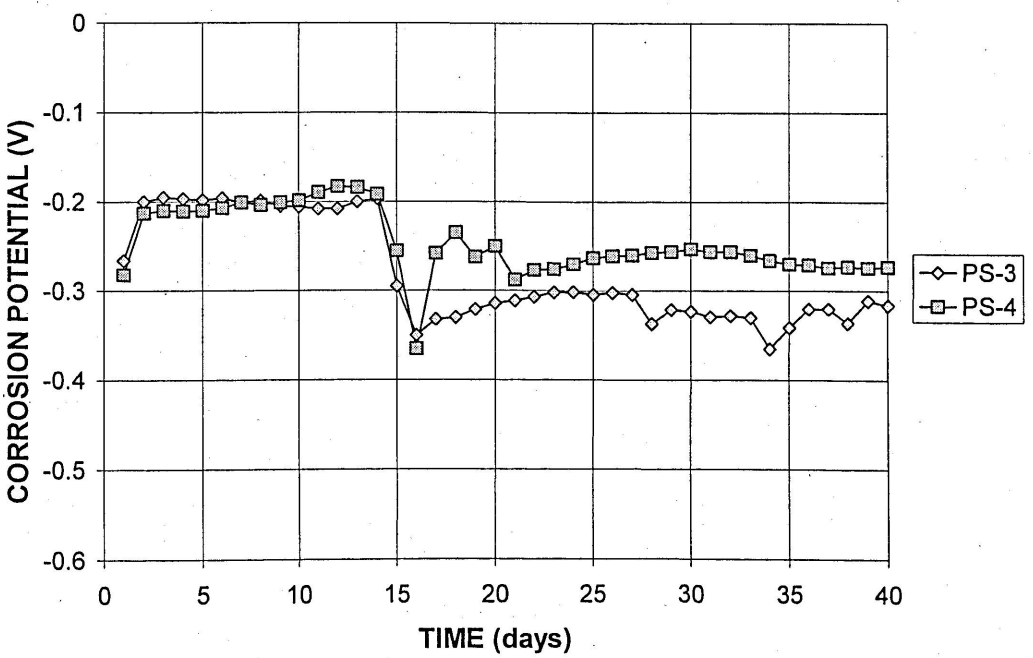

Figure 3.6 – Corrosion potential versus time for bare stainless steel clad bars with epoxy on the ends and exposed to 1.6 m NaCl in simulated pore solution: Specimens PS-3, PS-4

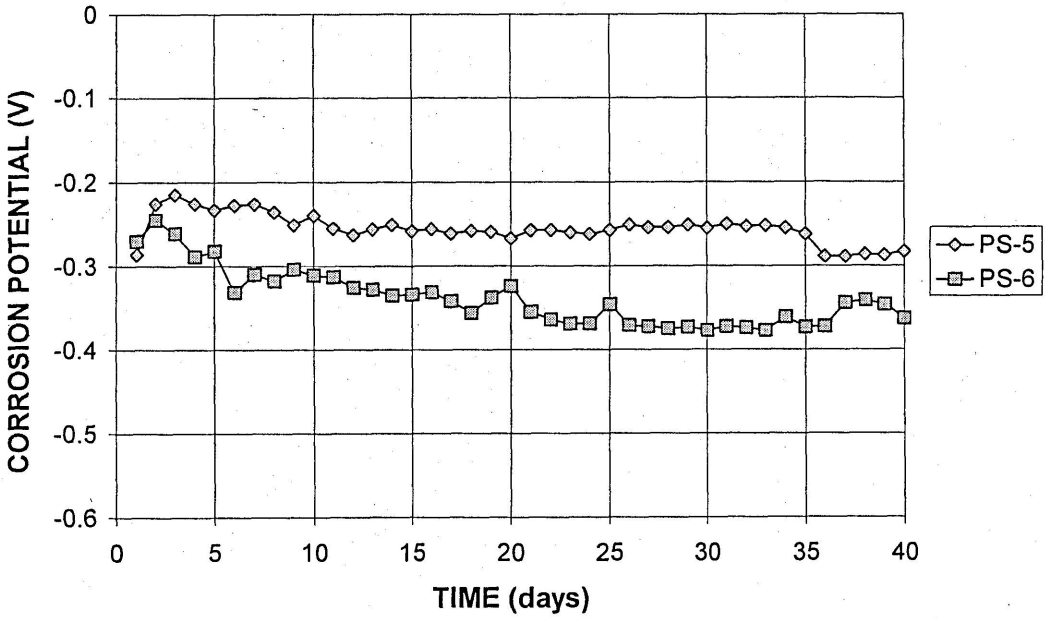

Figure 3.7 – Corrosion potential versus time for bare stainless steel clad bars with epoxy on the ends and exposed to 1.6 m NaCl in simulated pore solution: Specimens PS-5, PS-6

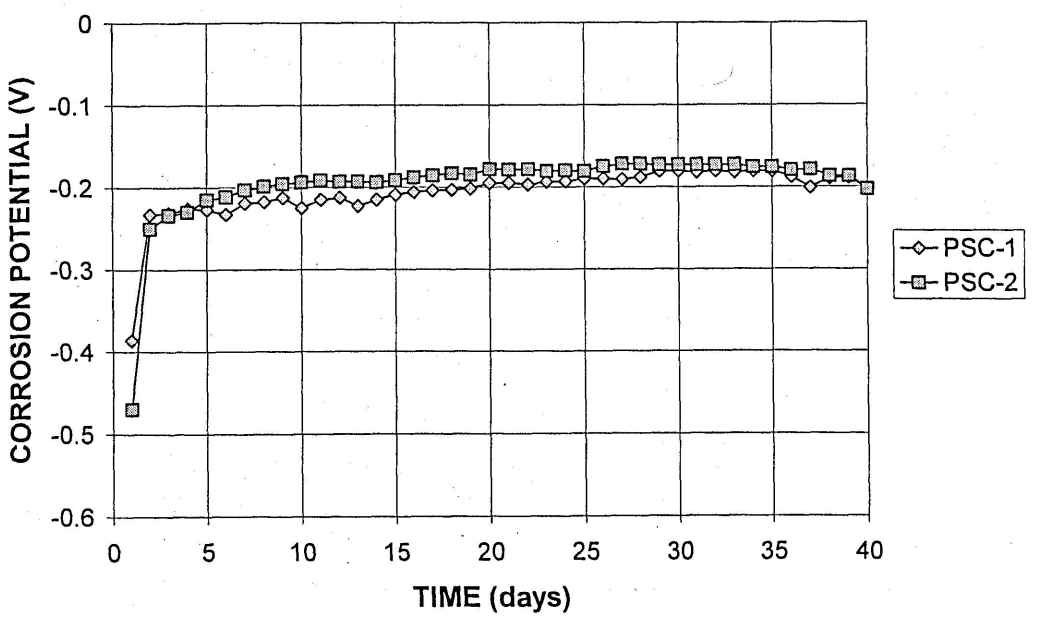

Figure 3.8 – Corrosion potential versus time for bare stainless steel clad bars with caps exposed to 1.6 m NaCl in simulated pore solution: Specimens PSC-1, PSC-2

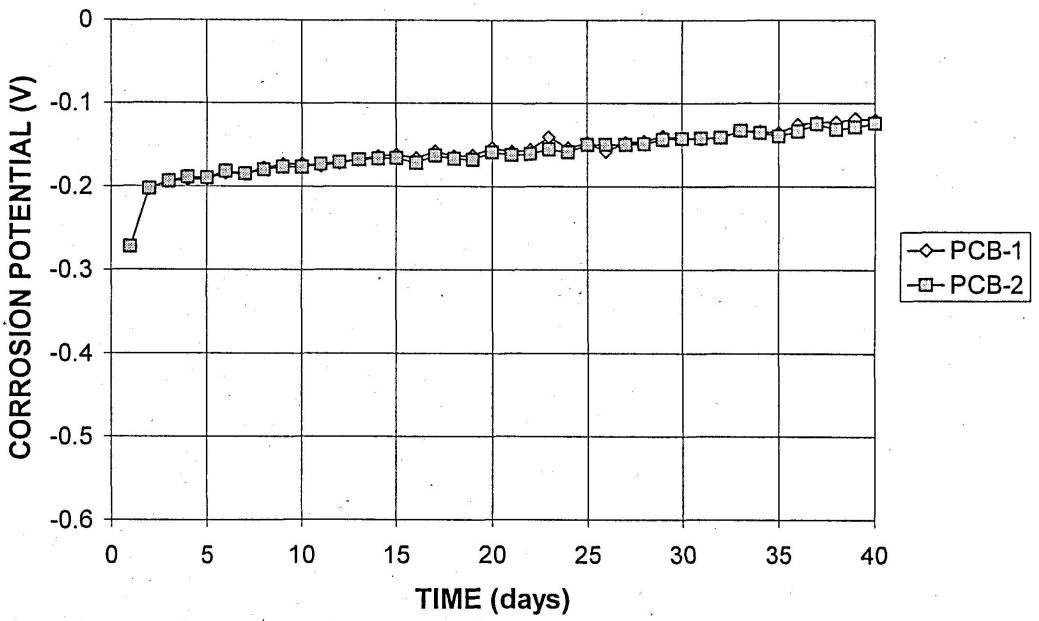

Figure 3.9 – Corrosion potential versus time for bare conventional steel bars with epoxy on the ends and in simulated pore solution: Specimens PCB-1 and PCB-2

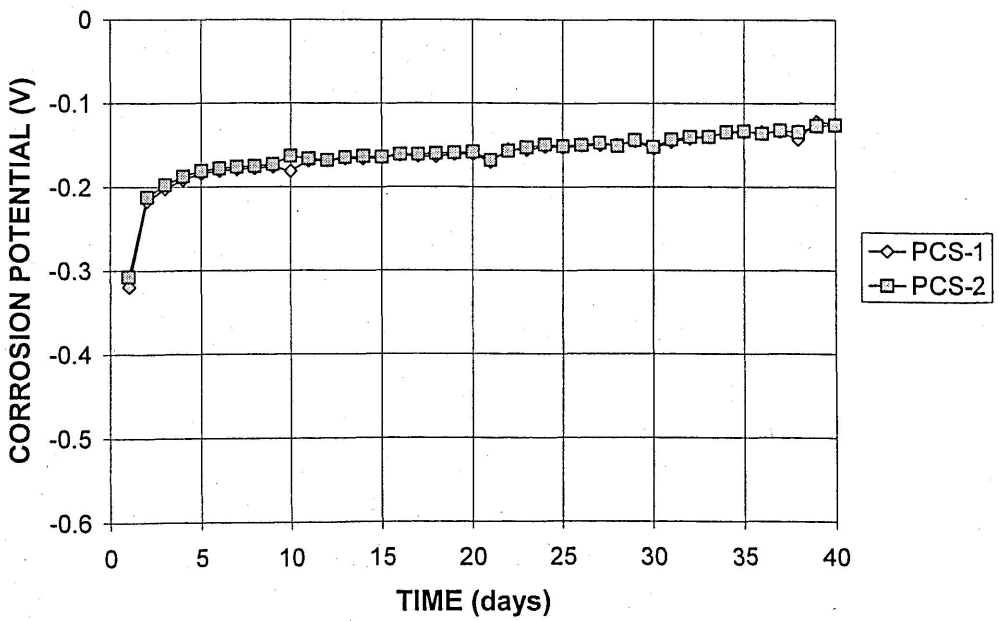

Figure 3.10 – Corrosion potential versus time for bare stainless steel clad bars with epoxy on the ends and in simulated pore solution: Specimens PCS-1, PCS-2

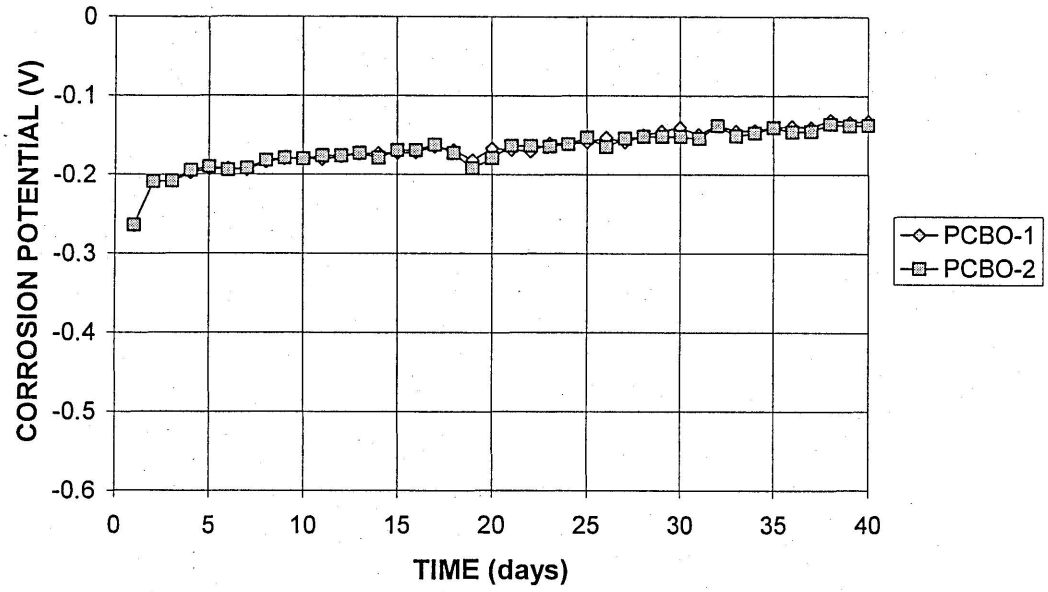

Figure 3.11 – Corrosion potential versus time for bare conventional steel bars with epoxy on the ends and exposed to simulated pore solution with scrubbed air pumped into the pore solution: Specimens PCBO-1 and PCBO-2

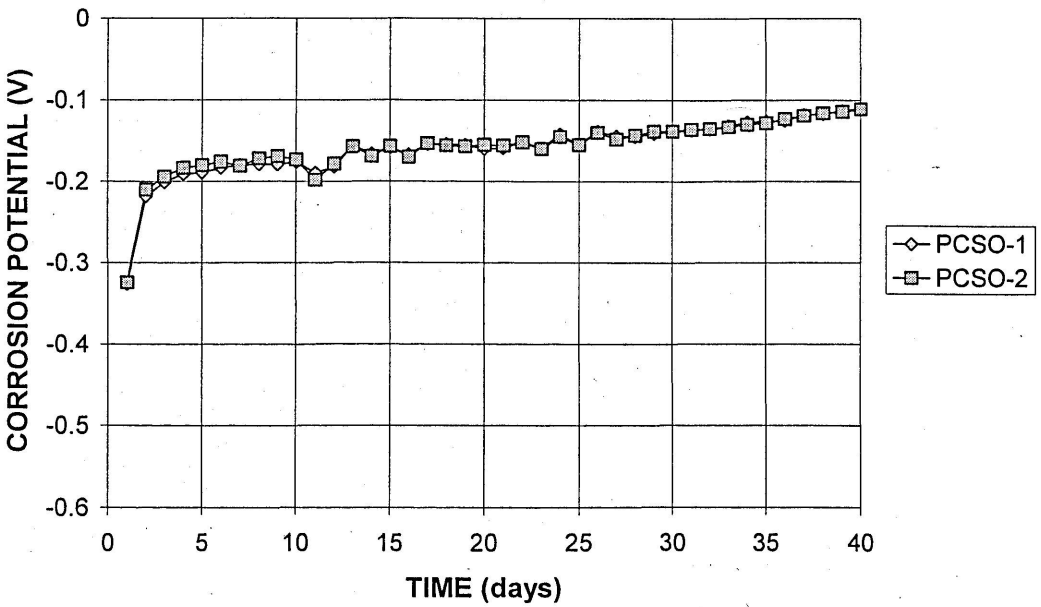

Figure 3.12 – Corrosion potential versus time for bare stainless steel clad bars with epoxy on the ends and exposed to simulated pore solution with scrubbed air pumped into the pore solution: Specimens PCSO-1 and PCSO-2

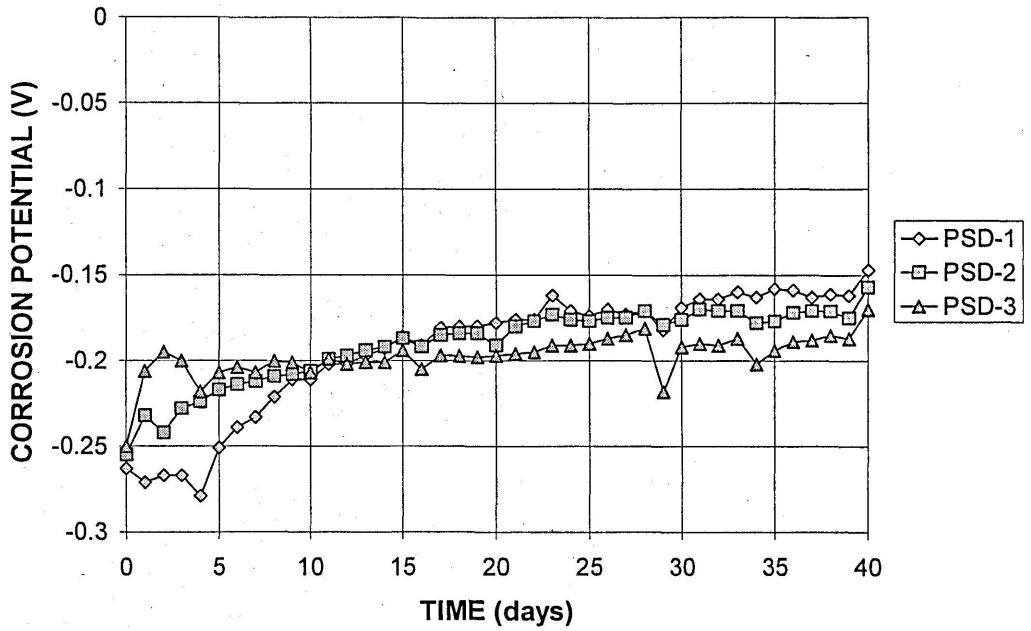

Figure 3.13 – Corrosion potential versus time for bare stainless steel clad bars with caps and a hole penetrating cladding exposed to 1.6 m NaCl in simulated pore solution: Specimens PSD-1, PSD-2, and PSD-3

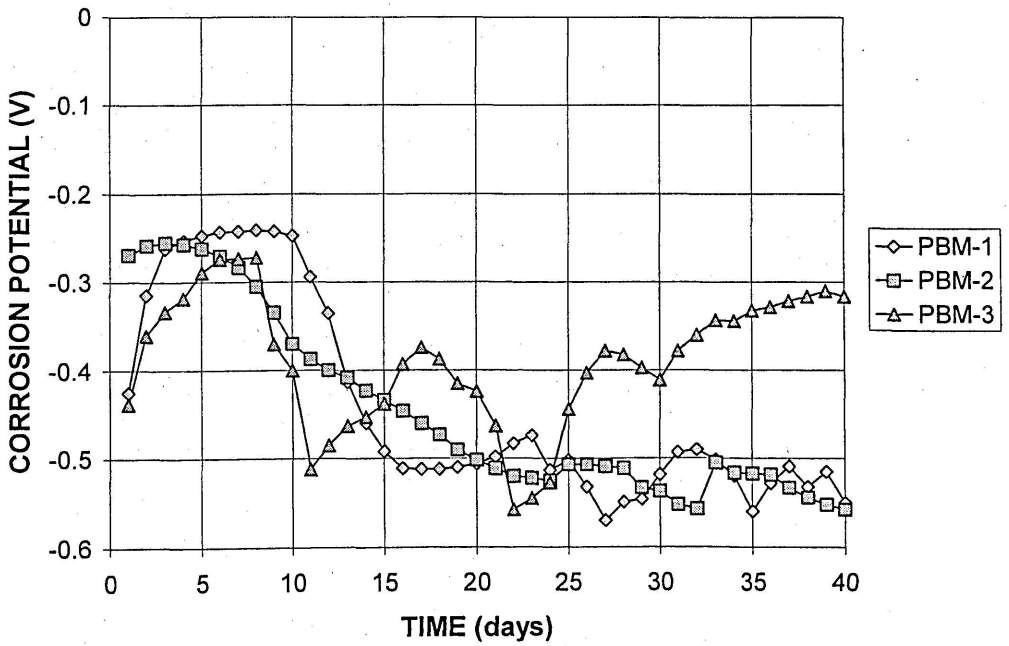

Figure 3.14 – Corrosion potential versus time for conventional steel bars with mortar covering exposed to 1.6 m NaCl in simulated pore solution: Specimens PBM-1, PBM-2 and PBM-3

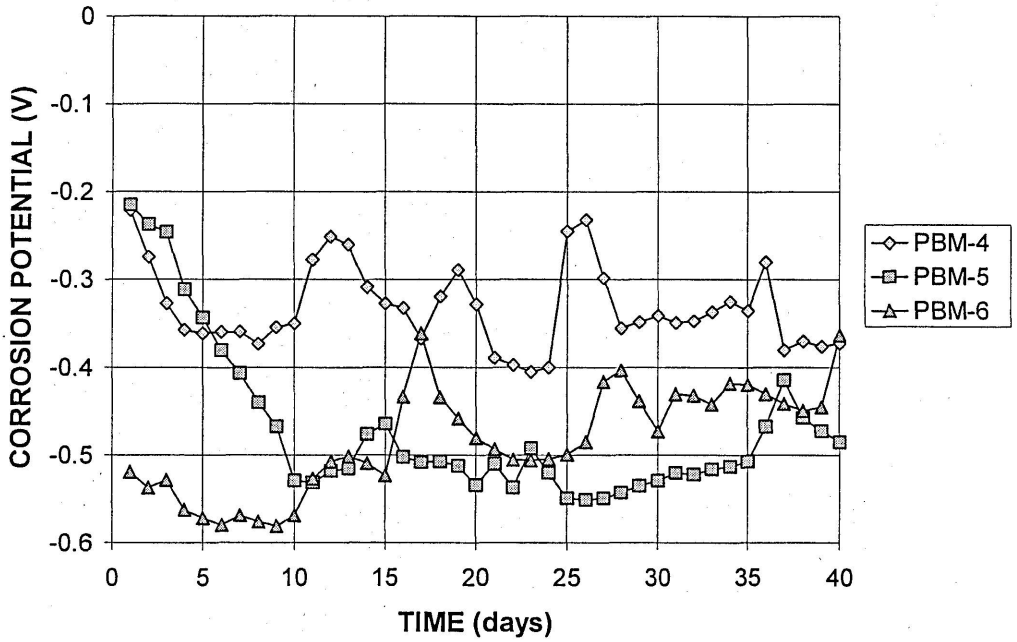

Figure 3.15 – Corrosion potential versus time for conventional steel bars with mortar covering exposed to 1.6 m NaCl in simulated pore solution: Specimens PBM-4, PBM-5, and PBM-6

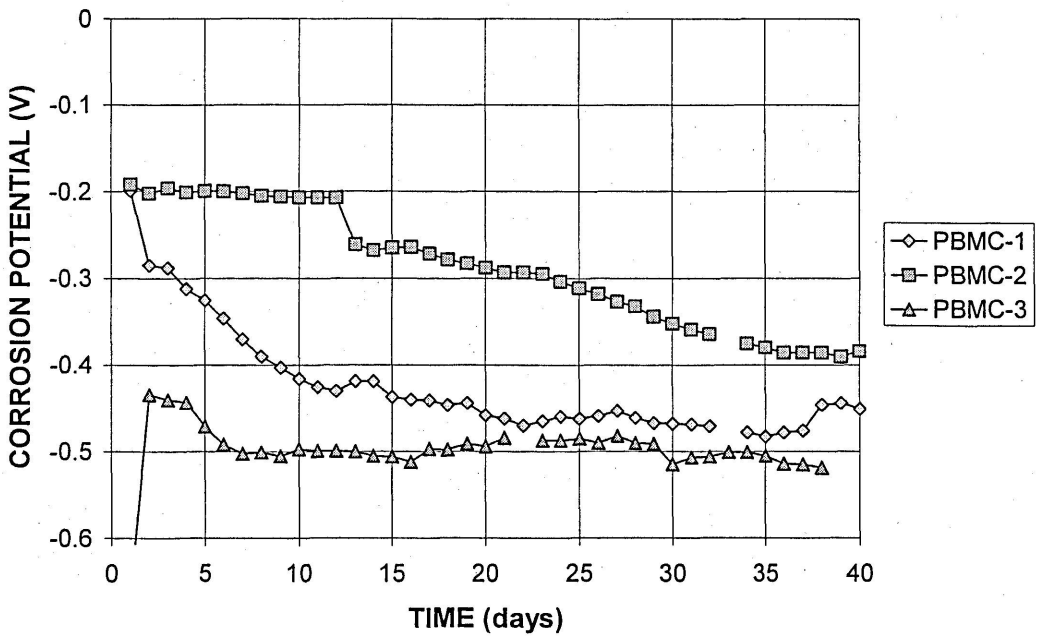

Figure 3.16 – Corrosion potential versus time for conventional steel bars with mortar covering and caps exposed to 1.6 m NaCl in simulated pore solution: Specimens PBMC-1, PBMC-2, and PBMC-3

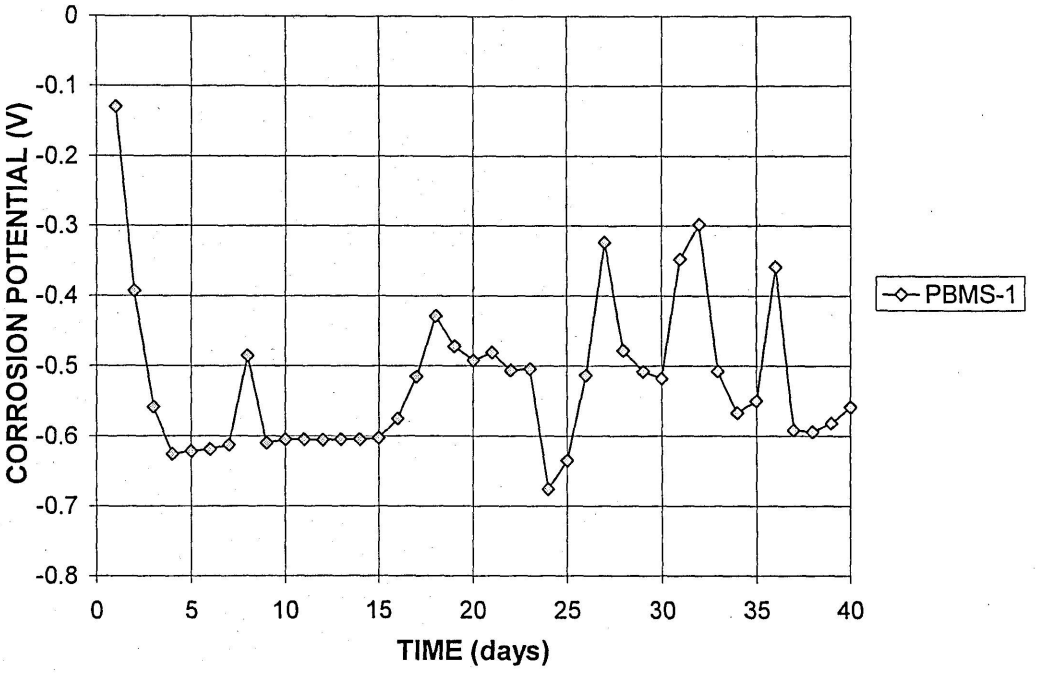

Figure 3.17 – Corrosion potential versus time for conventional steel bars with a reduced thickness mortar cover exposed to 1.6 m NaCl in simulated pore solution: Specimens PBMS-1

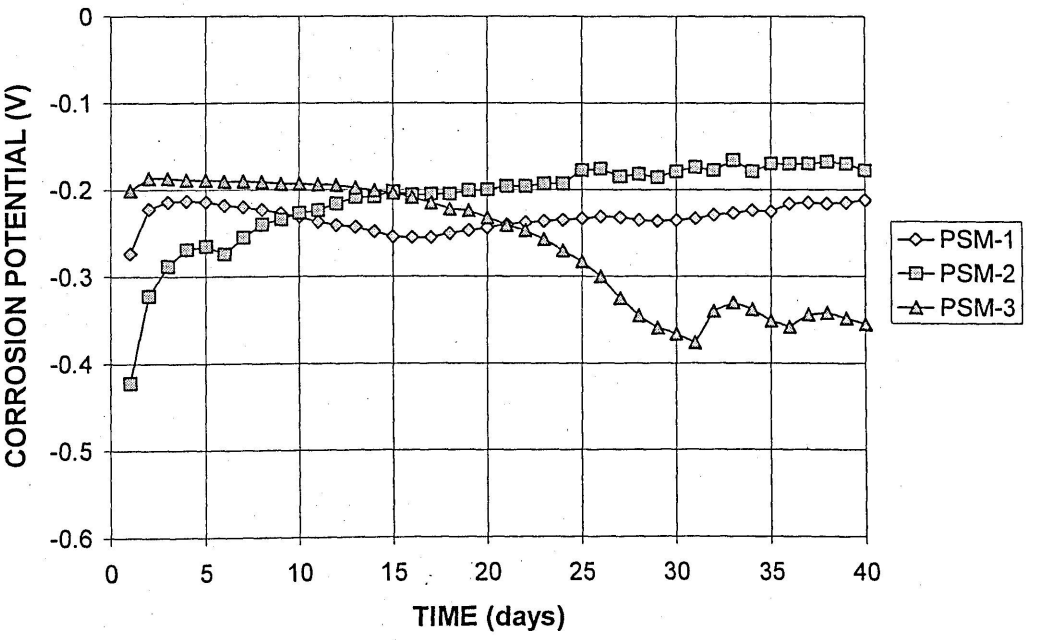

Figure 3.18 – Corrosion potential versus time for stainless steel clad bars with mortar covering exposed to 1.6 m NaCl in simulated pore solution: Specimens PSM-1, PSM-2, and PSM-3

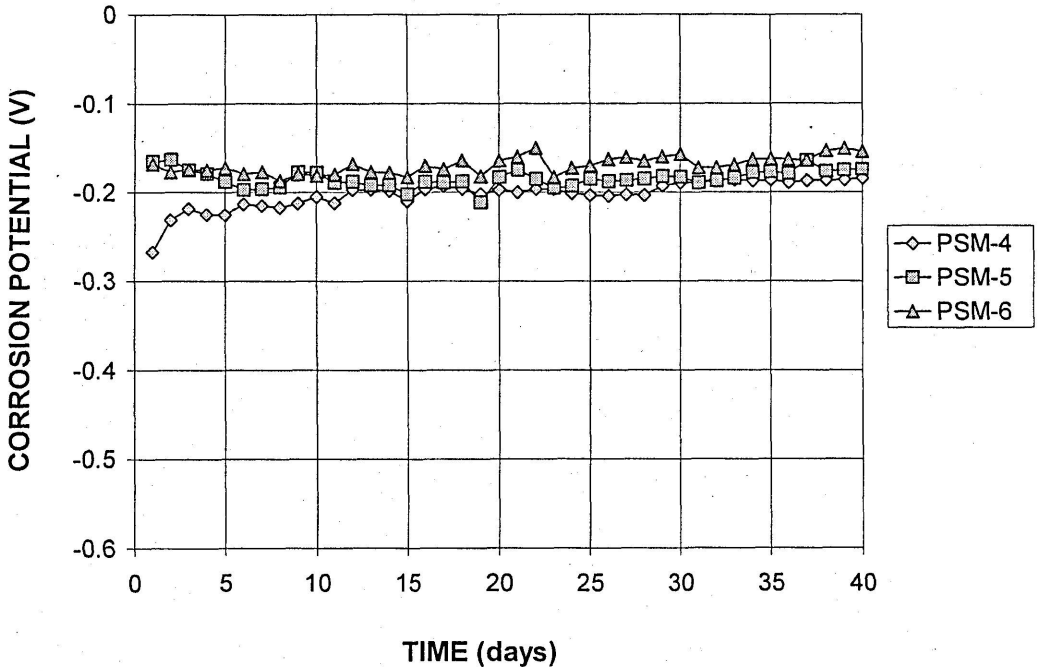

Figure 3.19 – Corrosion potential versus time for stainless steel clad bars with mortar covering exposed to 1.6 m NaCl in simulated pore solution: Specimens PSM-4, PSM-5, and PSM-6

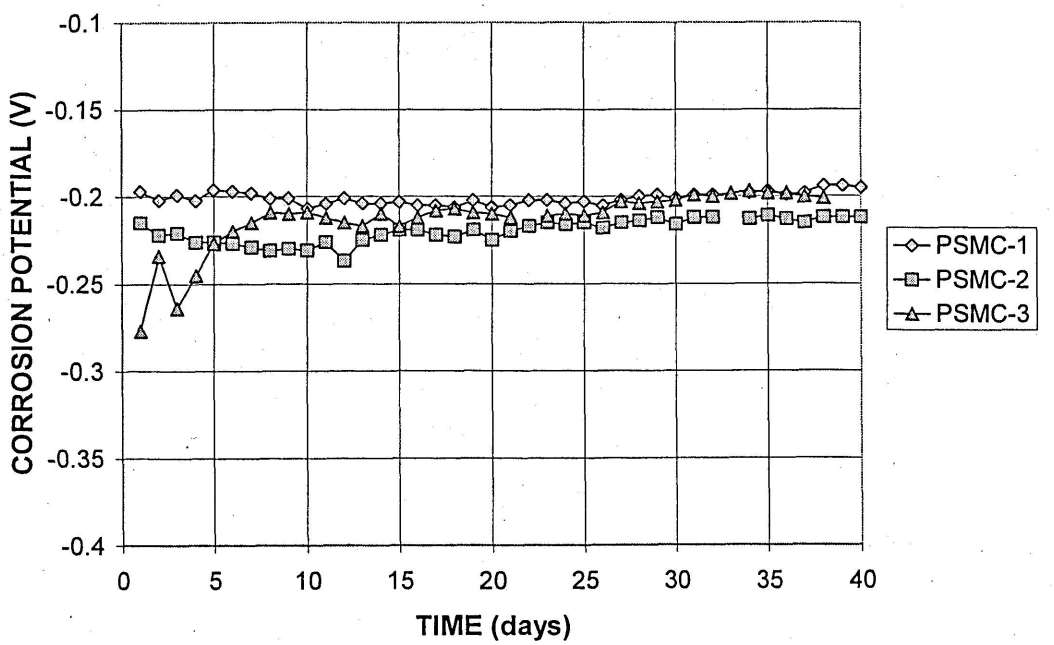

Figure 3.20 – Corrosion potential versus time for stainless steel clad bars with mortar covering and caps exposed to 1.6 m NaCl in simulated pore solution: Specimens PSMC-1, PSMC-2, and PSMC-3

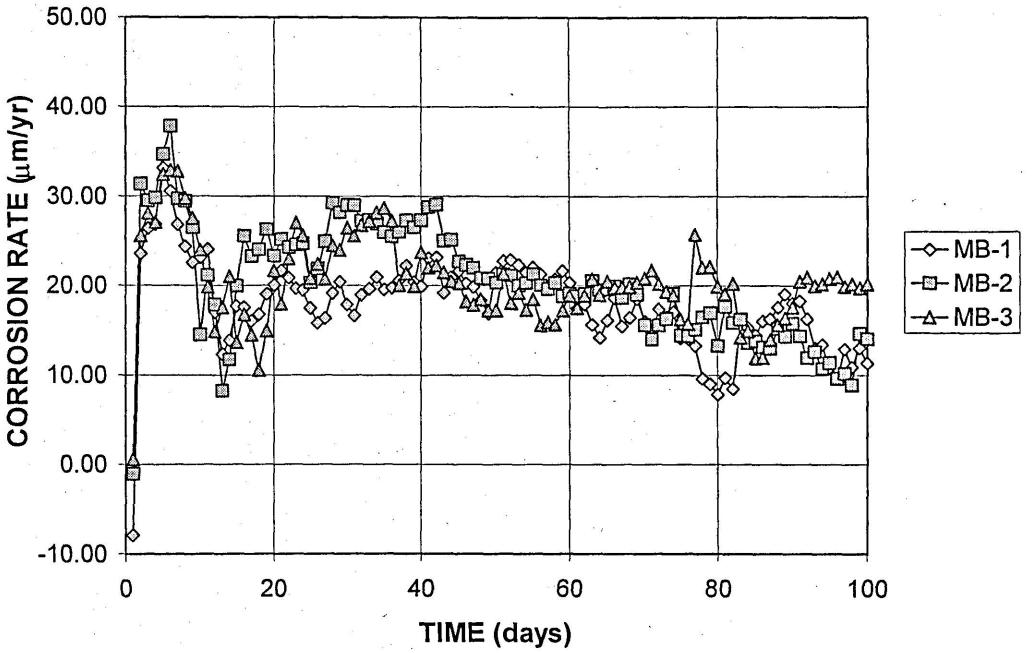

Figure 3.21 – Macrocell corrosion rate versus time for bare conventional steel bars with epoxy at the ends and exposed to 1.6 m NaCl in simulated pore solution: Specimens MB-1, MB-2, and MB-3

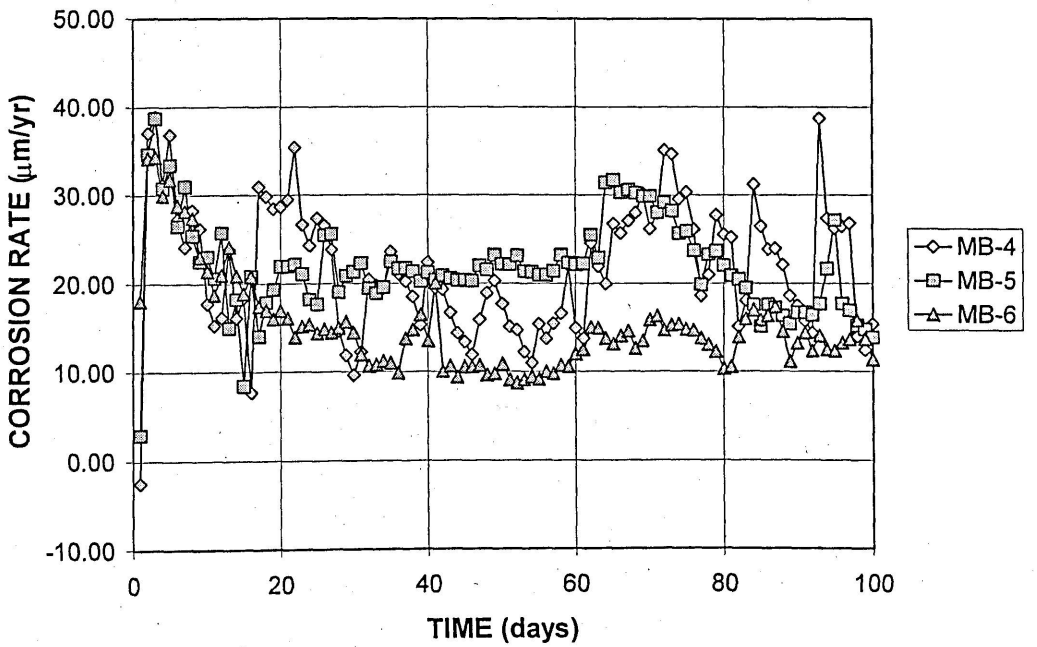

Figure 3.22 – Macrocell corrosion rate versus time for bare conventional steel bars with epoxy on the ends and exposed to 1.6 m NaCl in simulated pore solution: Specimens MB-4, MB-5, and MB-6

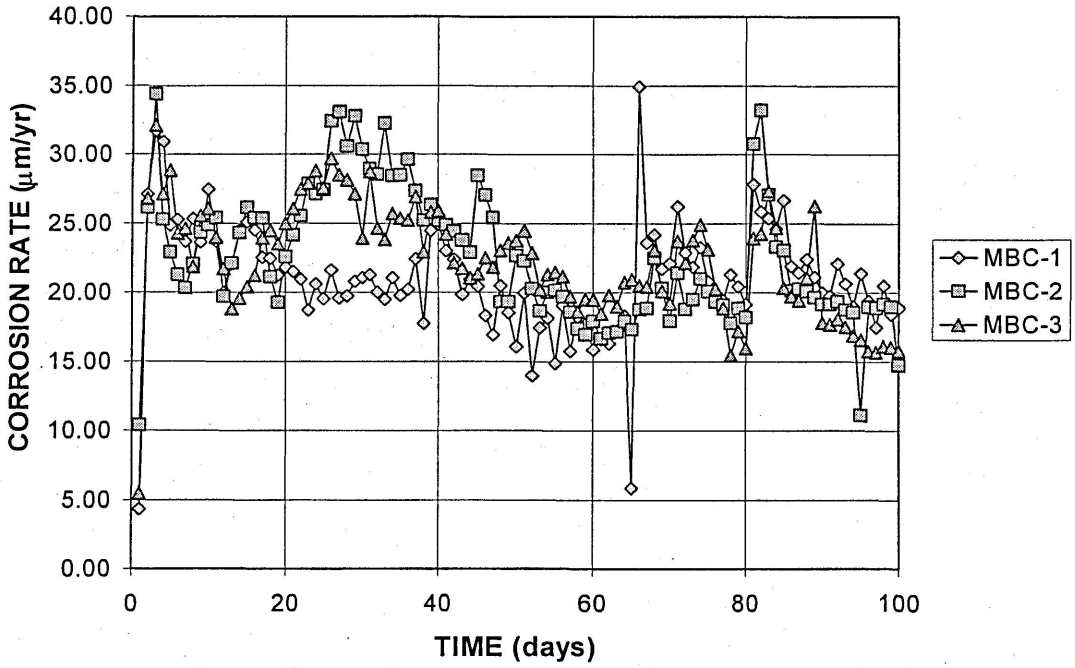

Figure 3.23 – Macrocell corrosion rate versus time for bare conventional steel bars with caps exposed to 1.6 m NaCl in simulated pore solution: Specimens MBC-1, MBC-2, and MBC-3

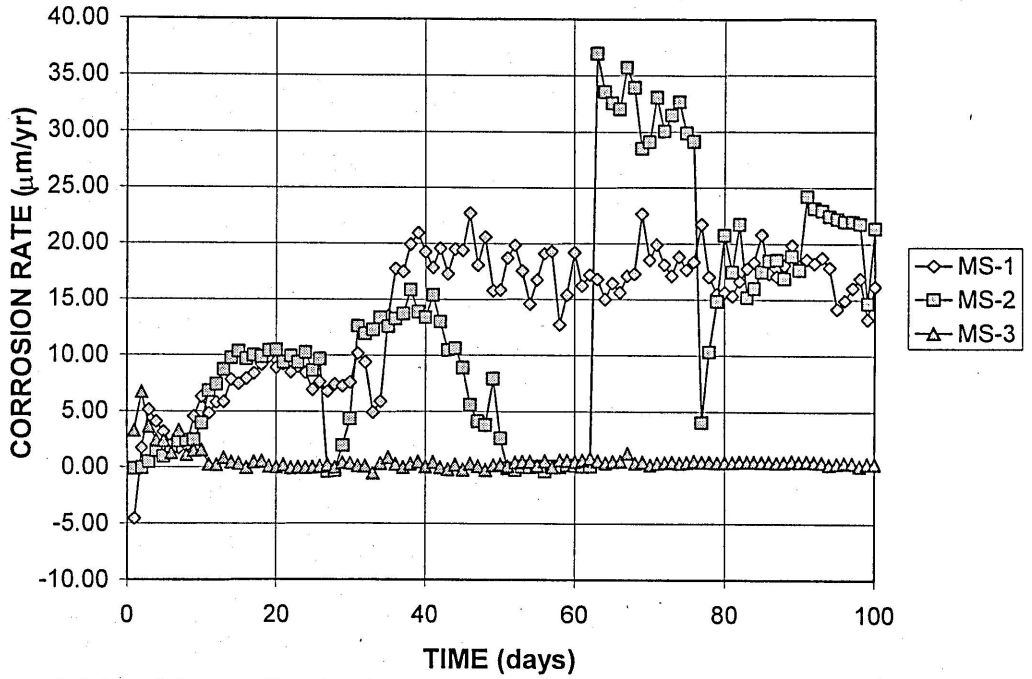

Figure 3.24a – Macrocell corrosion rate versus time for bare stainless steel clad bars with epoxy on the ends and exposed to 1.6 m NaCl in simulated pore solution: Specimens MS-1, MS-2, and MS-3

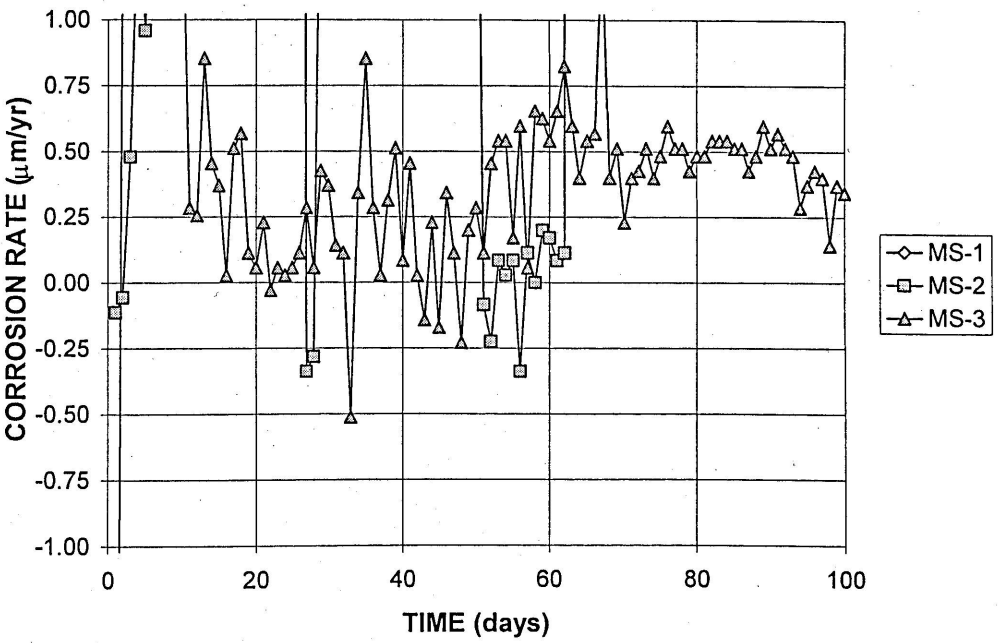

Figure 3.24b – Macrocell corrosion rate versus time for bare stainless steel clad bars with epoxy on the ends and exposed to 1.6 m NaCl in simulated pore solution: Specimens MS-1, MS-2, and MS-3

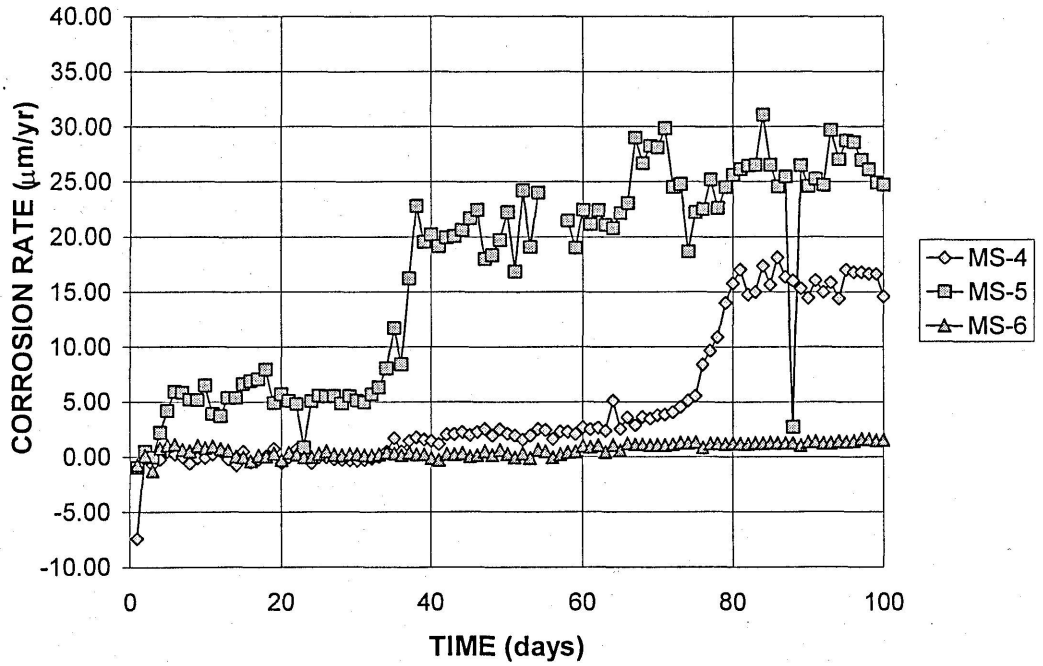

Figure 3.25a – Macrocell corrosion rate versus time for bare stainless steel clad bars with epoxy on the ends and exposed to 1.6 m NaCl in simulated pore solution: Specimens MS-4, MS-5, and MS-6

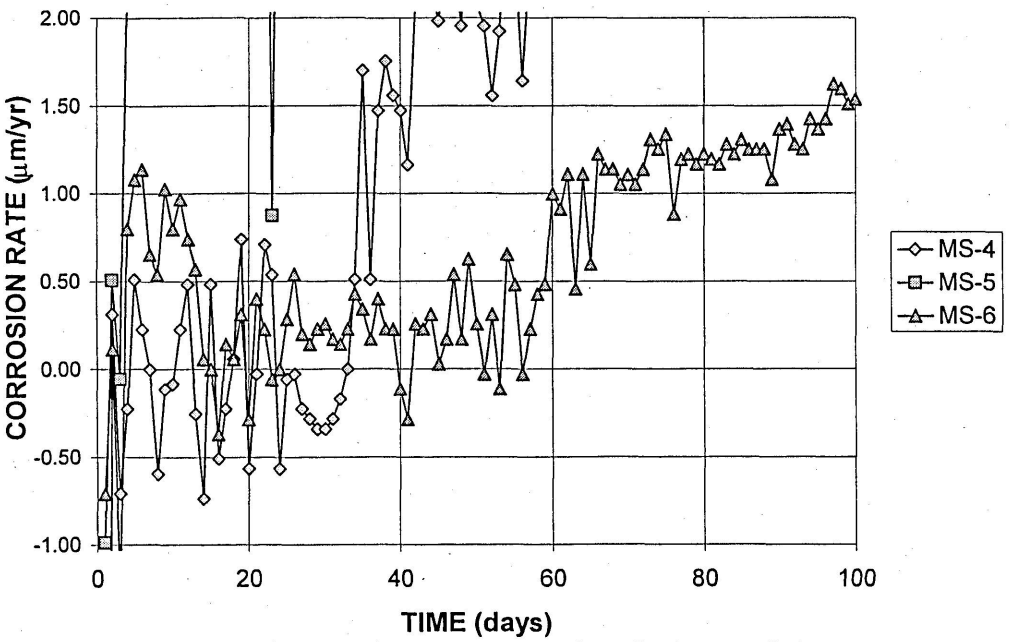

Figure 3.25b – Macrocell corrosion rate versus time for bare stainless steel clad bars with epoxy on the ends and exposed to 1.6 m NaCl in simulated pore solution: Specimens MS-4, MS-5, and MS-6

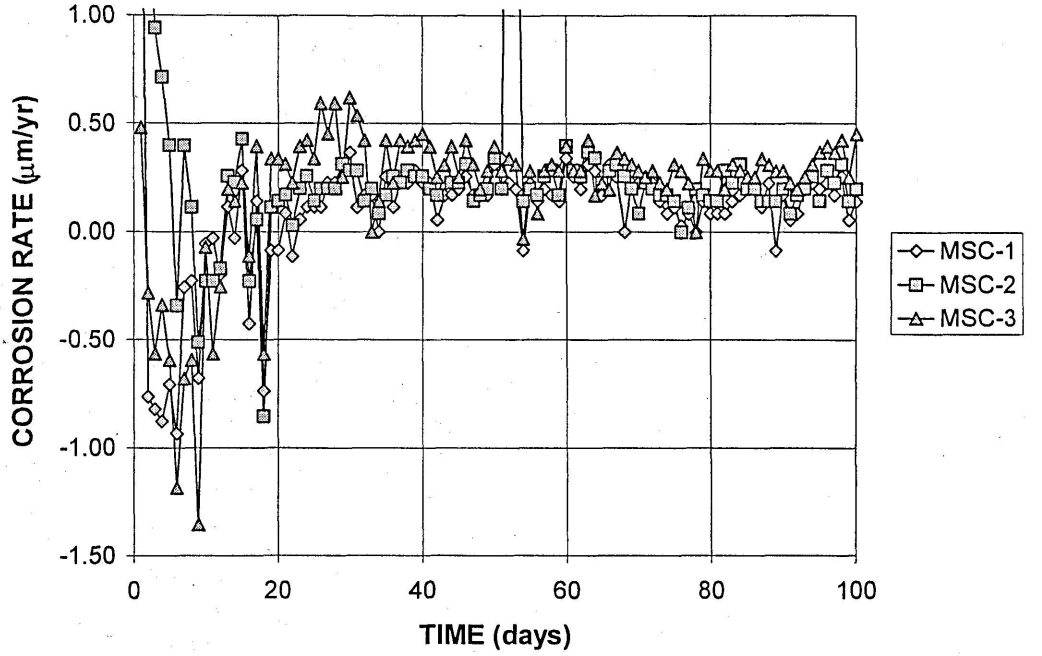

Figure 3.26 – Macrocell corrosion rate versus time for bare stainless steel clad bars with caps exposed to 1.6 m NaCl in simulated pore solution: Specimens MSC-1, MSC-2, and MSC-3

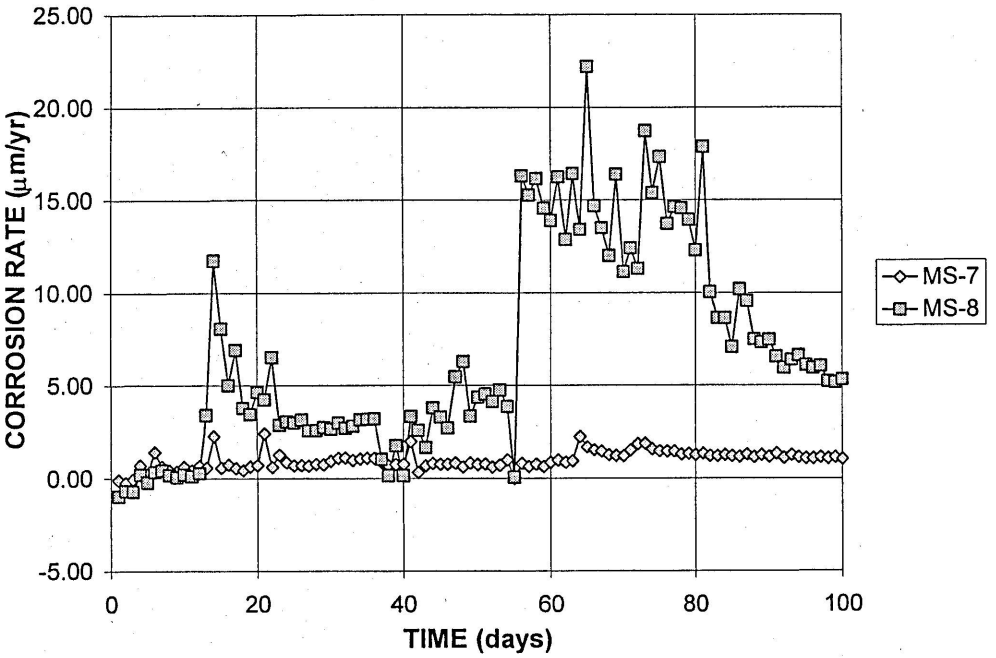

Figure 3.27a – Macrocell corrosion rate versus time for sandblasted bare stainless steel clad bars with epoxy on the ends and exposed to 1.6 m NaCl in simulated pore solution: Specimens MS-7, MS-8

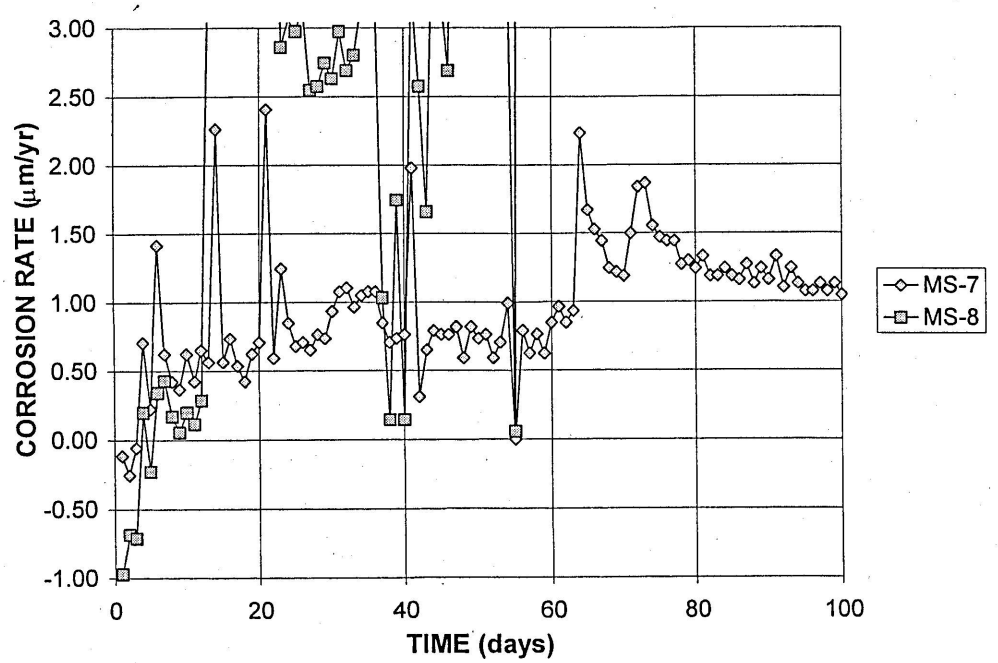

Figure 3.27b – Macrocell corrosion rate versus time for sandblasted bare stainless steel clad bars with epoxy on the ends and exposed to 1.6 m NaCl in simulated pore solution: Specimens MS-7, MS-8

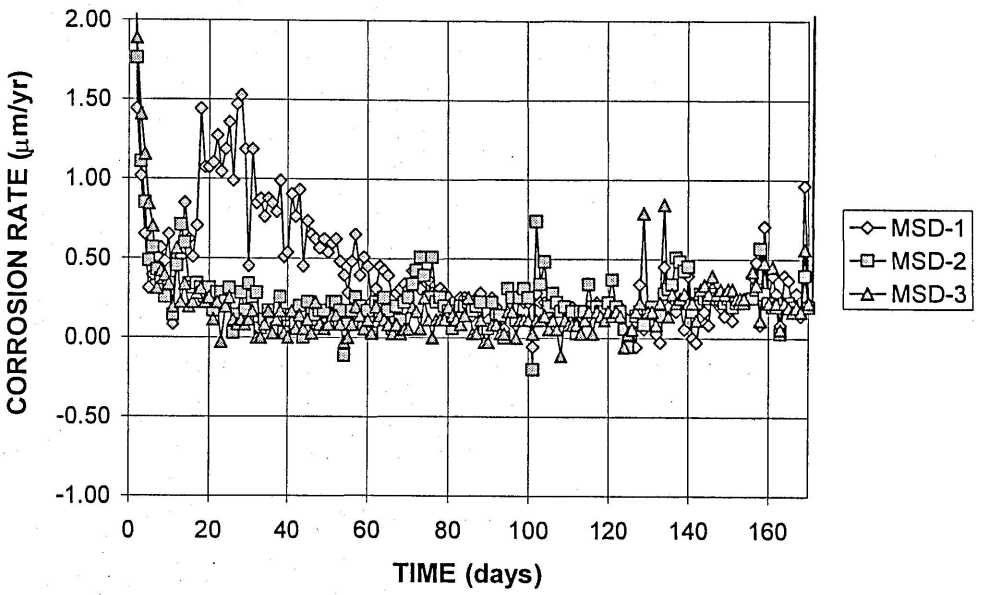

Figure 3.28 – Macrocell corrosion rate versus time for bare stainless steel clad bars with caps and with a hole penetrating cladding exposed to 1.6 m NaCl in simulated pore solution: Specimens MSD-1, MSD-2, and MSD-3

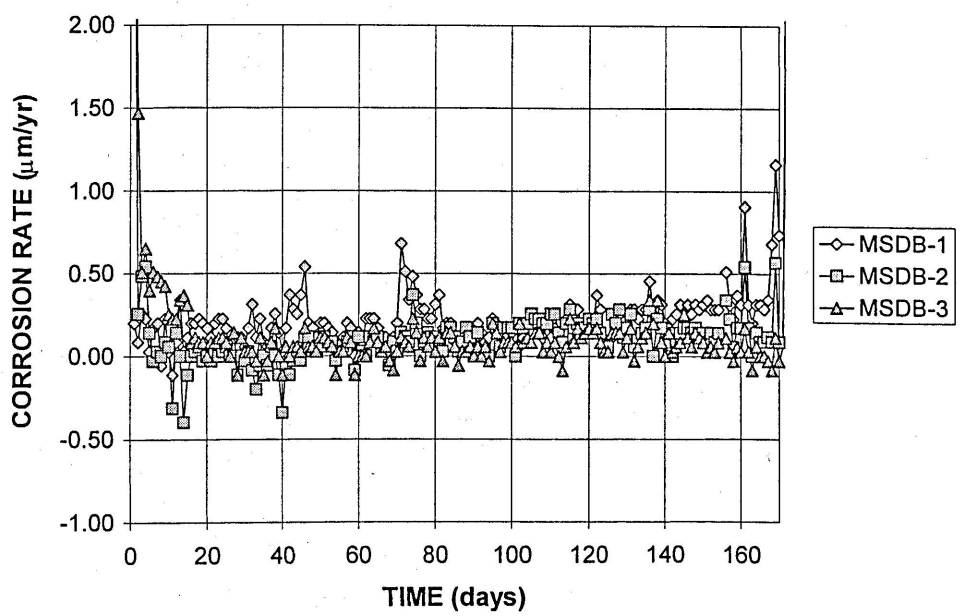

Figure 3.29 – Macrocell corrosion rate versus time for bare stainless steel clad bars with hole penetrating cladding and connected to conventional steel cathode exposed to 1.6 m NaCl in simulated pore solution: Specimens MSDB-1, MSDB-2, and MSDB-3

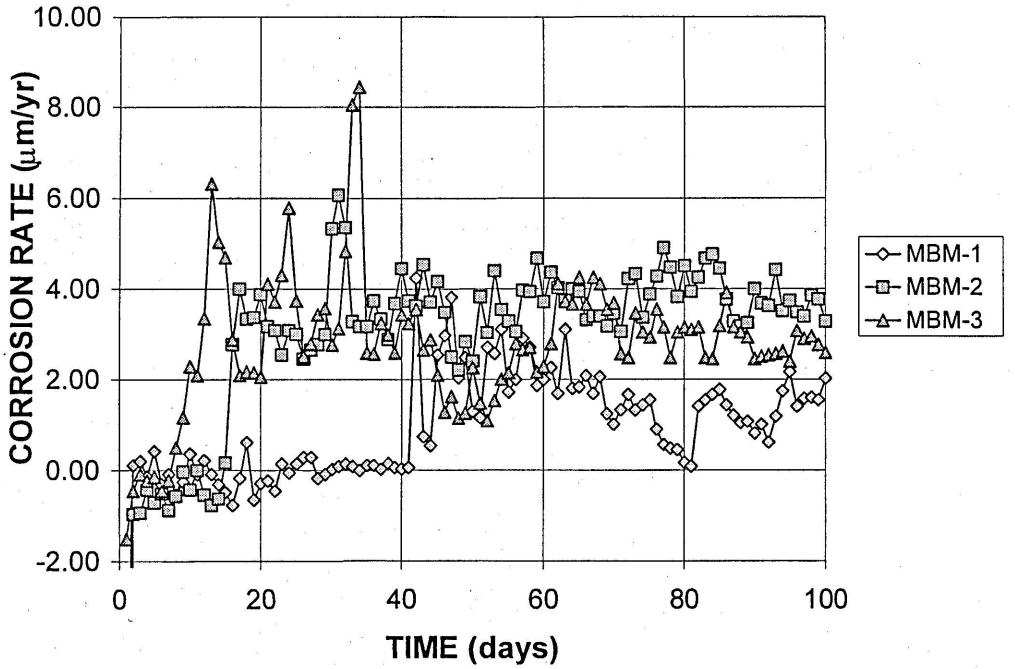

Figure 3.30 – Macrocell corrosion rate versus time for conventional steel bars with mortar covering exposed to 1.6 m NaCl in simulated pore solution: Specimens MBM-1, MBM-2, and MBM-3

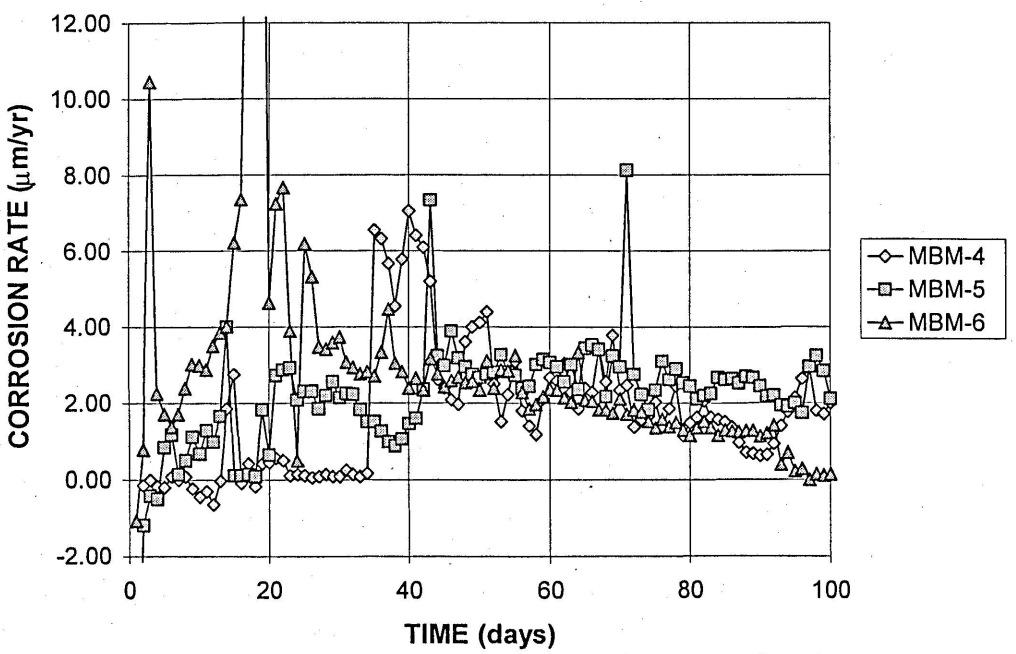

Figure 3.31 – Macrocell corrosion rate versus time for conventional steel bars with mortar covering exposed to 1.6 m NaCl in simulated pore solution: Specimens MBM-4, MBM-5, and MBM-6

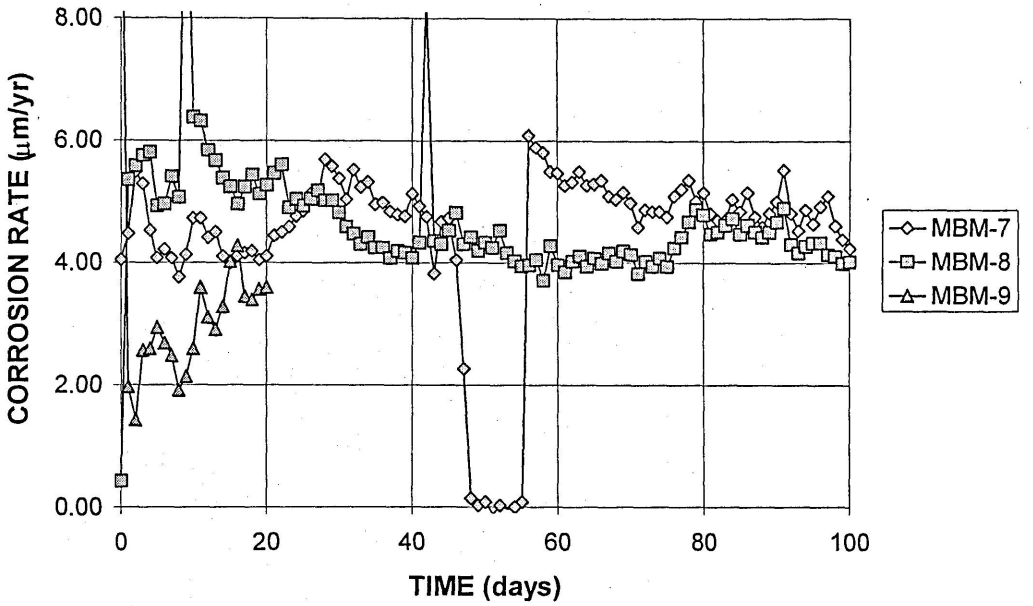

Figure 3.32 – Macrocell corrosion rate versus time for conventional steel bars with mortar covering exposed to 1.6 m NaCl in simulated pore solution: Specimens MBM-7, MBM-8, and MBM-9

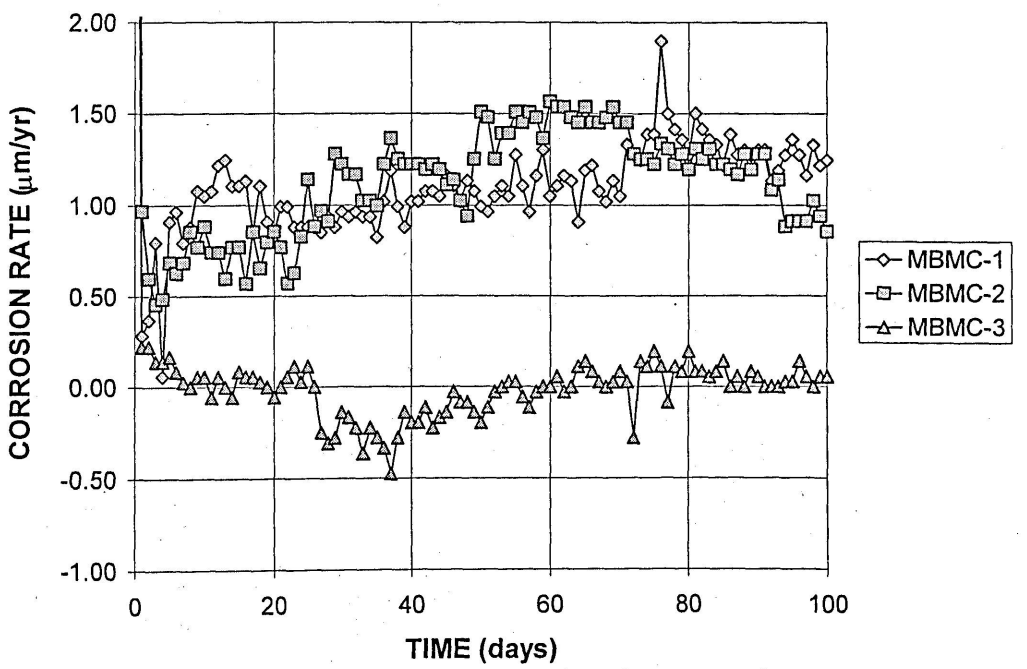

Figure 3.33 – Macrocell corrosion rate versus time for conventional steel bars with mortar covering and caps exposed to 1.6 m NaCl in simulated pore solution: Specimens MBMC-1, MBMC-25, and MBMC-3

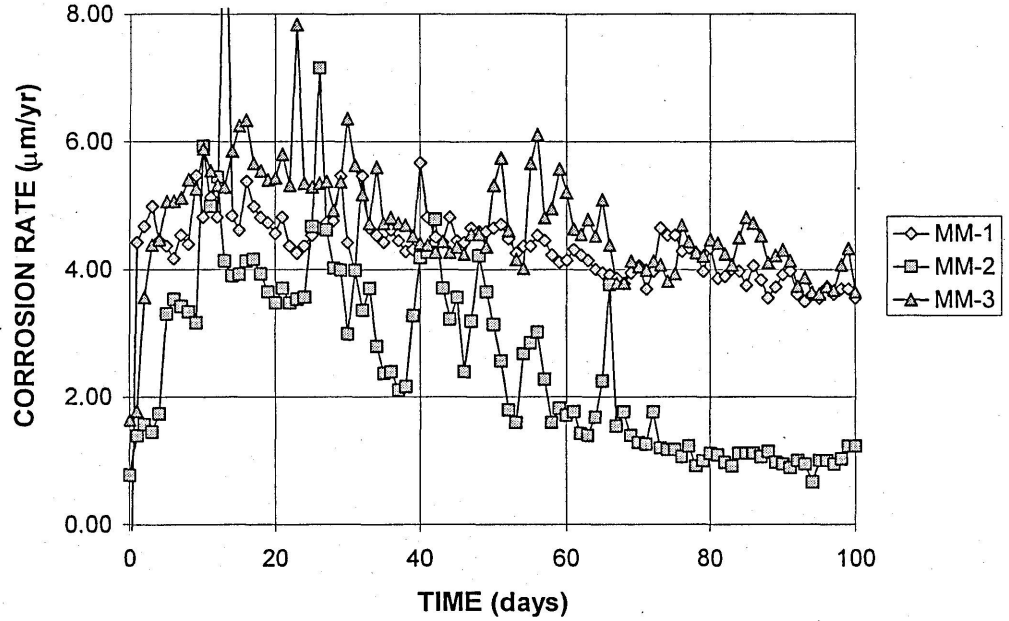

Figure 3.34 – Macrocell corrosion rate versus time for conventional steel bars with mortar covering and connected to bare conventional steel cathode exposed to 1.6 m NaCl in simulated pore solution: Specimens MM-1, MM-2, and MM-3

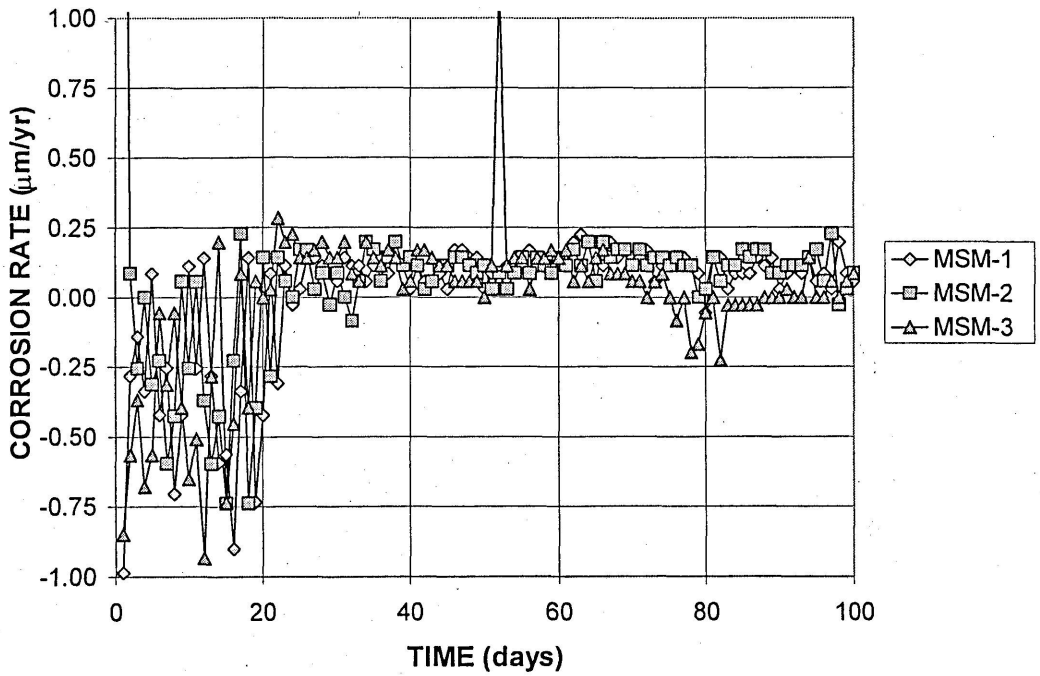

Figure 3.35 – Macrocell corrosion rate versus time for stainless steel clad bars with mortar covering exposed to 1.6 m NaCl in simulated pore solution: Specimens MSM-1, MSM-2, and MSM-3

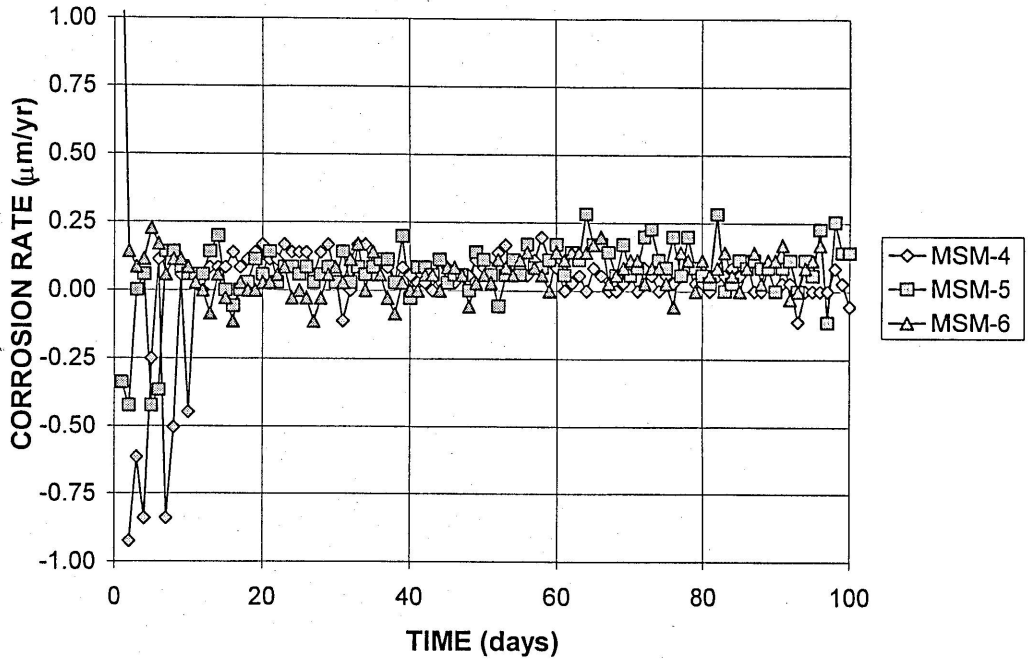

Figure 3.36 – Macrocell corrosion rate versus time for stainless steel clad bars with mortar covering exposed to 1.6 m NaCl in simulated pore solution: Specimens MSM-4, MSM-5, and MSM-6

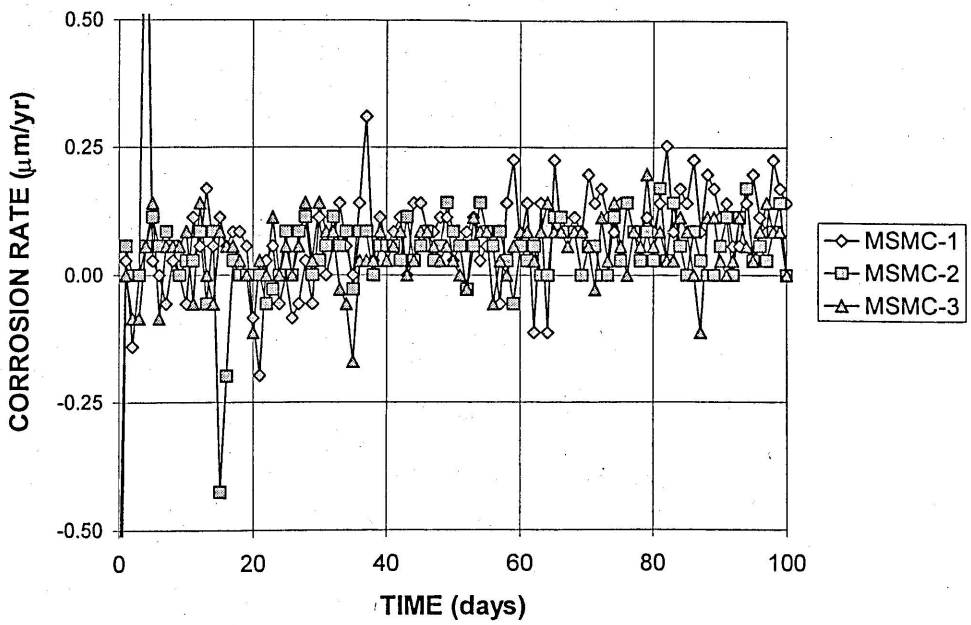

Figure 3.37 – Macrocell corrosion rate versus time for stainless steel clad bars with mortar covering and caps exposed to 1.6 m NaCl in simulated pore solution: Specimens MSMC-1, MSMC-2, and MSMC-3

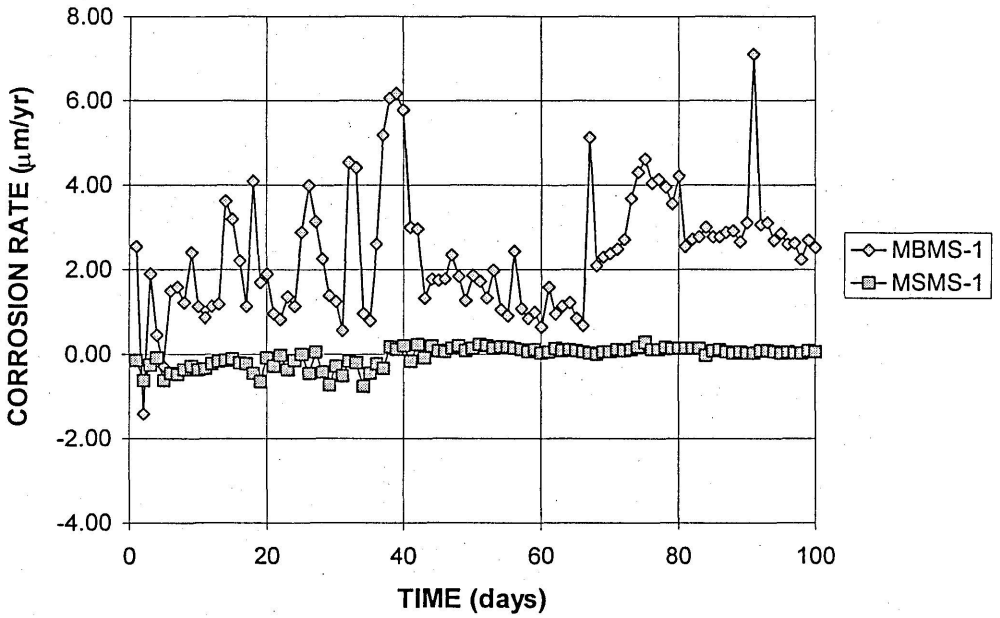

Figure 3.38a – Macrocell corrosion rate versus time for stainless steel clad and conventional bars with a reduced thickness mortar cover and with caps exposed to 1.6 m NaCl in simulated pore solution: Specimens MBMS-1 and MSMS-1

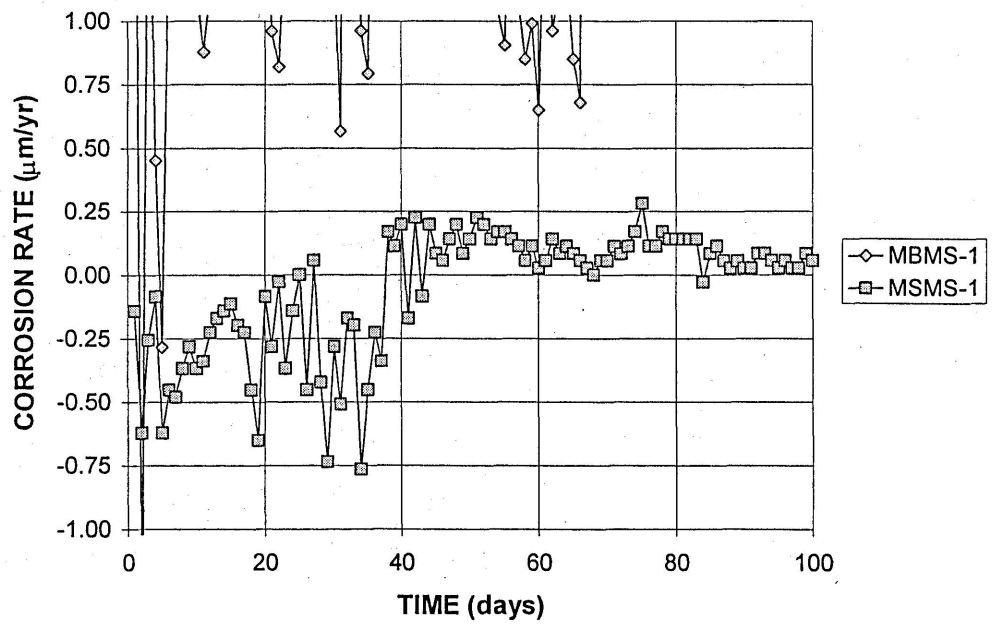

Figure 3.38b – Macrocell corrosion rate versus time for stainless steel clad and conventional bars with a reduced thickness mortar cover and with caps exposed to 1.6 m NaCl in simulated pore solution: Specimens MBMS-1 and MSMS-1

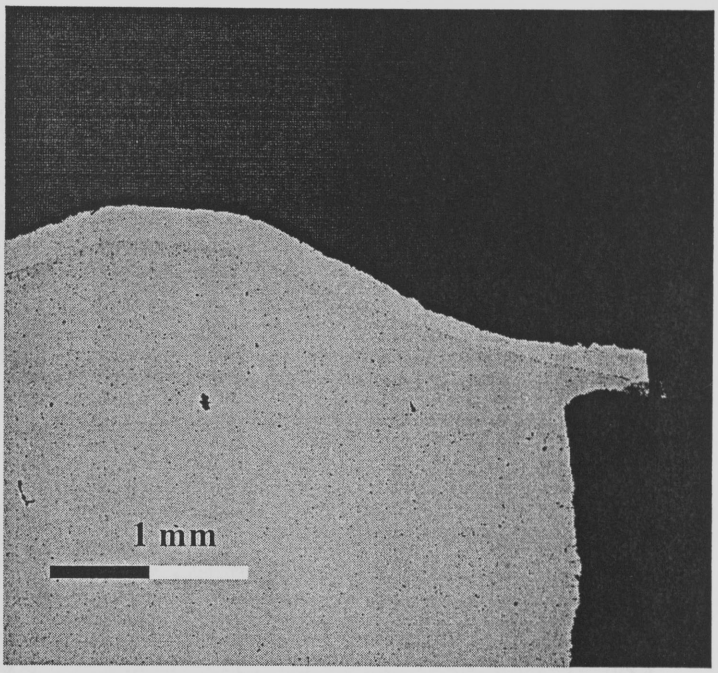

Figure 3.39 – Variation in stainless steel cladding thickness for longitudinally cut specimen

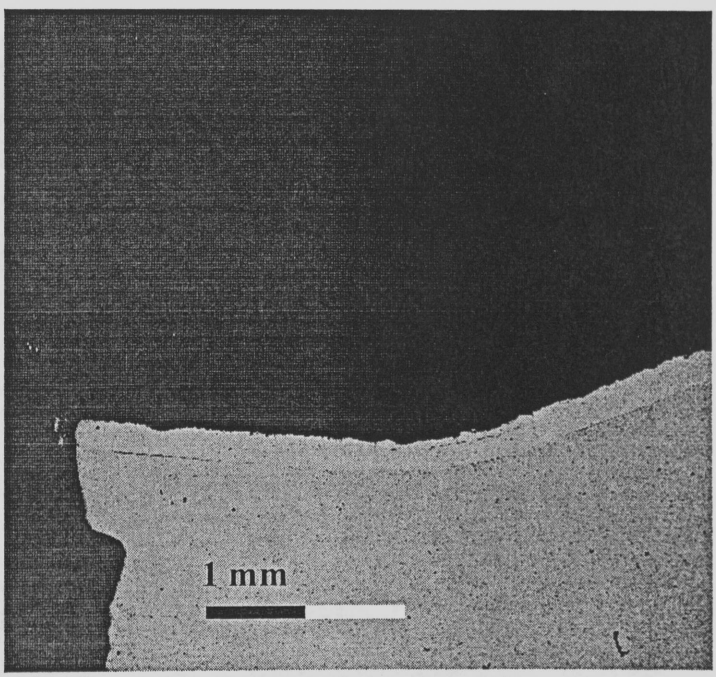

Figure 3.40 – Variation in stainless steel cladding thickness for the left side of the specimen shown in Figure 3.39

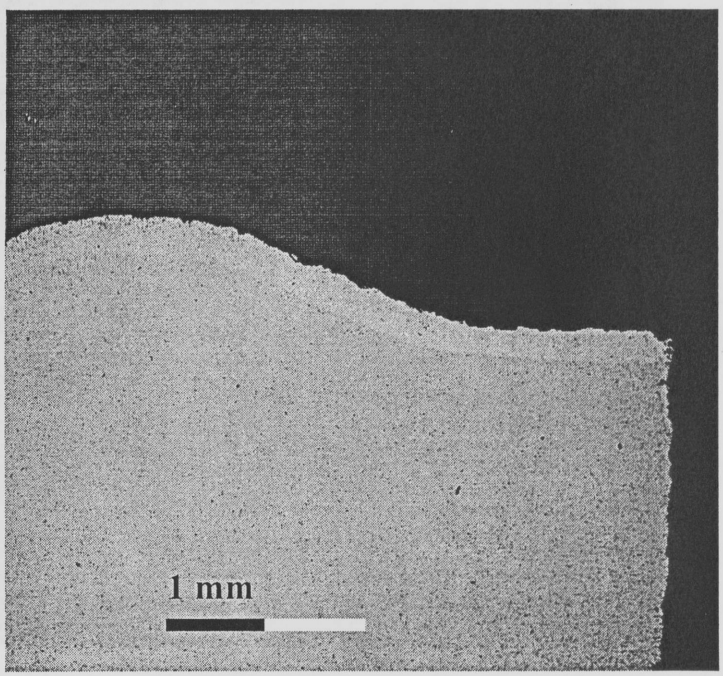

Figure 3.41 – Variation in stainless steel cladding thickness for longitudinally cut specimen

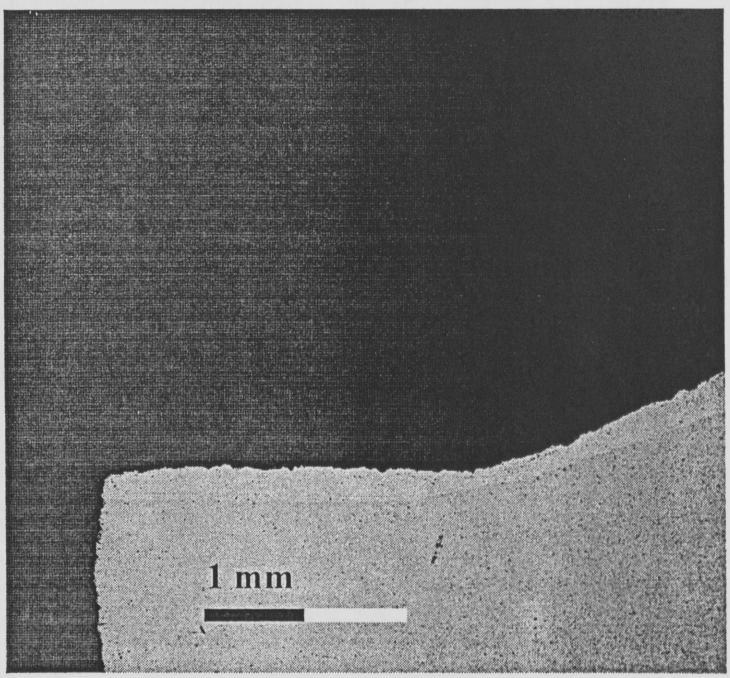

Figure 3.42 – Variation in stainless steel cladding thickness for the left side of the specimen shown in Figure 3.41

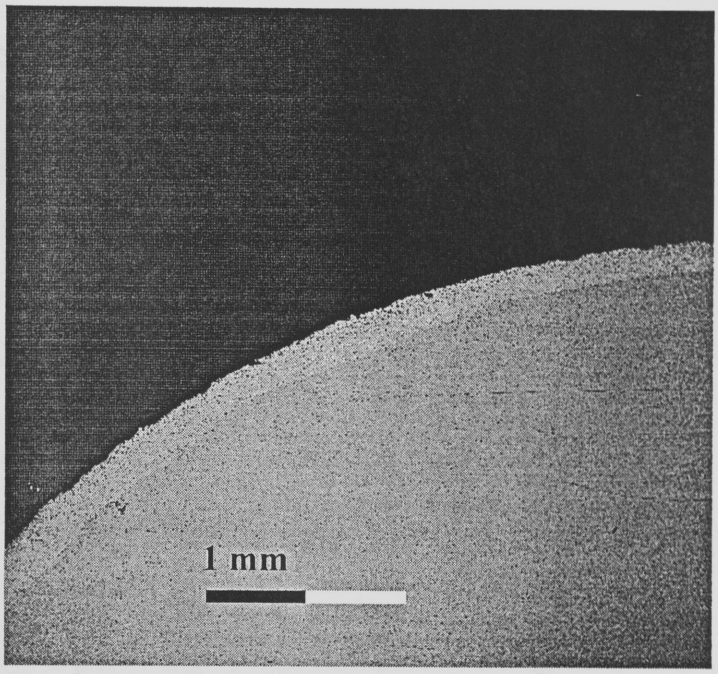

Figure 3.43 – Variation in stainless steel cladding thickness for transversely cut specimen

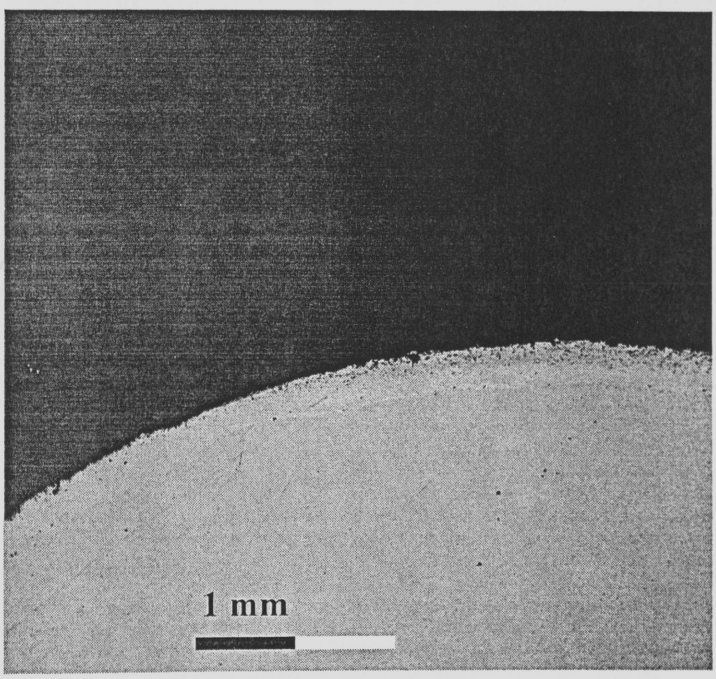

Figure 3.44 – Variation in stainless steel cladding thickness for transversely cut specimen

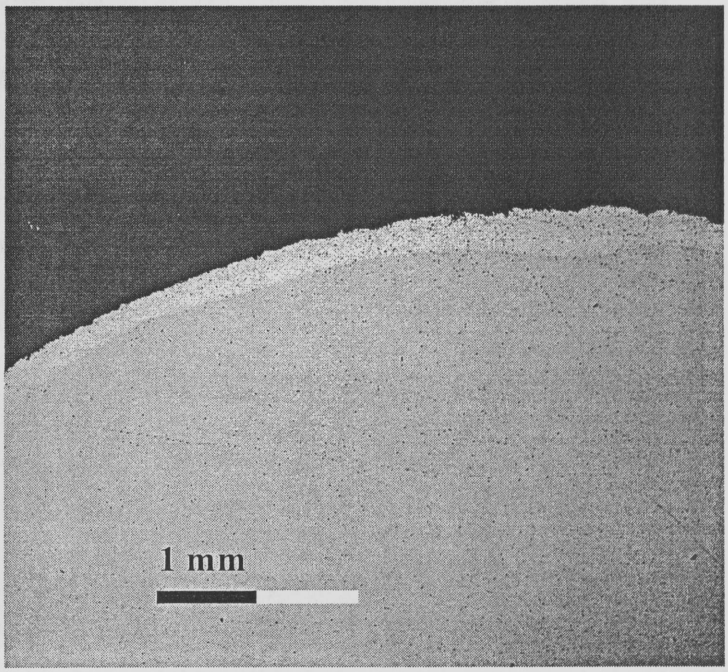

Figure 3.45 – Variation in stainless steel cladding thickness for transversely cut specimen

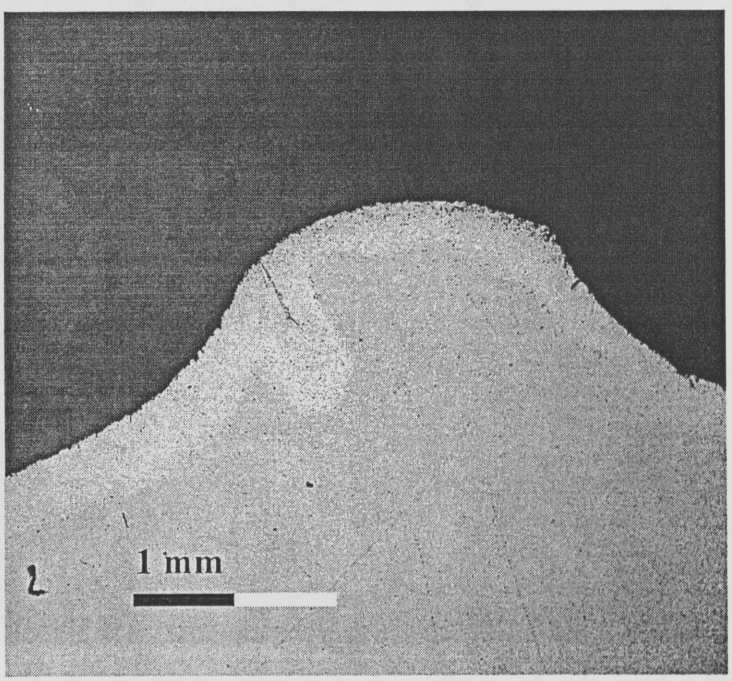

Figure 3.46 – Crack in stainless steel indention at longitudinal rib

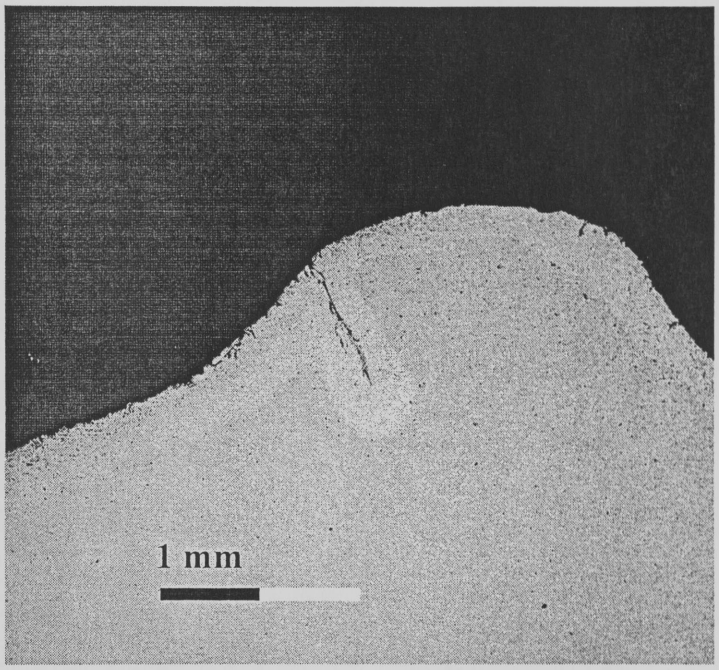

Figure 3.47 – Crack in stainless steel indention at longitudinal rib

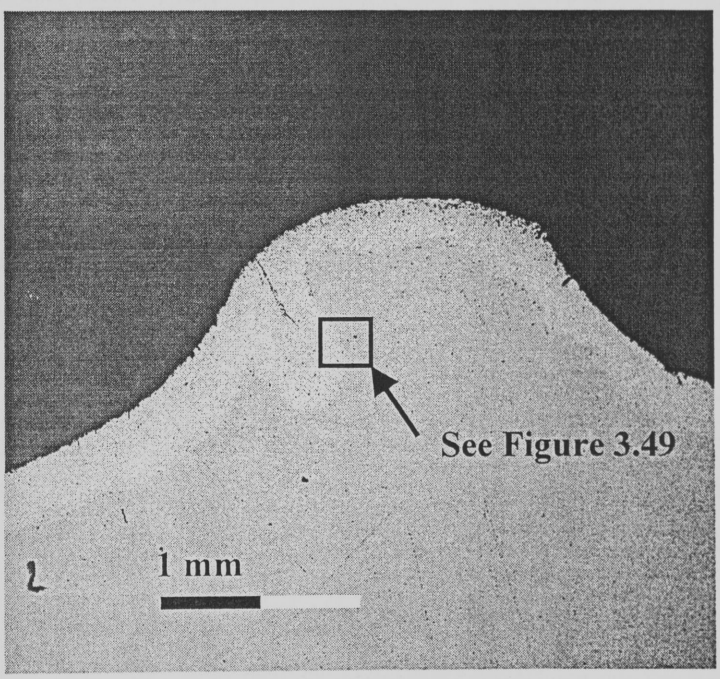

Figure 3.48 – Crack in stainless steel indention at longitudinal rib

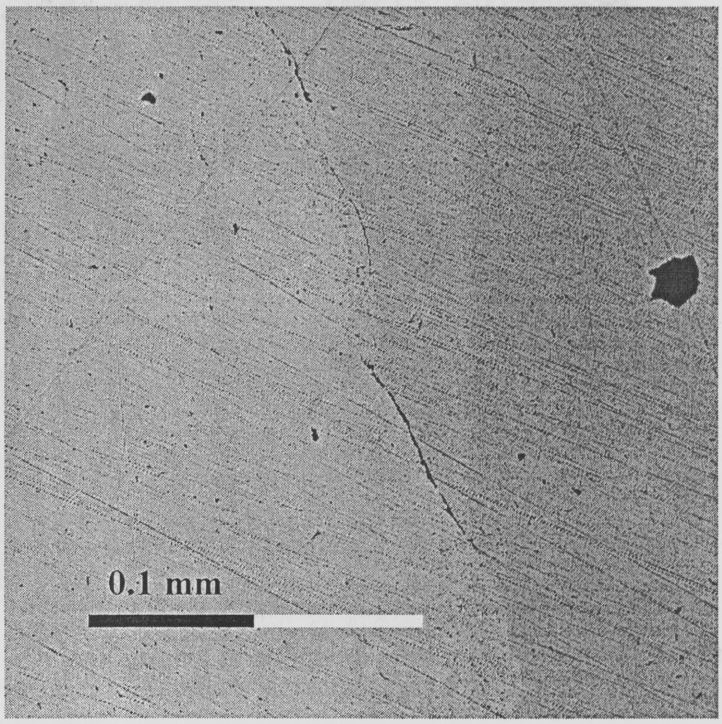

Figure 3.49 – Crack along interface between stainless steel cladding (at indentation) and mild steel. Region is shown in Figure 3.48. Crack thickness is approximately 1.5 μm.